PRODUCTION OF Z+JET EVENTS AND HF JET ENERGY SCALE CALIBRATION AT 7 TEV IN THE CMS EXPERIMENT AT LHC

A THESIS SUBMITTED TO
THE GRADUATE SCHOOL OF NATURAL AND APPLIED SCIENCES
OF
MIDDLE EAST TECHNICAL UNIVERSITY

BY

BUĞRA BİLİN

IN PARTIAL FULFILLMENT OF THE REQUIREMENTS
FOR
THE DEGREE OF MASTER OF SCIENCE
IN
PHYSICS

SEPTEMBER 2011

Approval of the thesis:

PRODUCTION OF Z+JET EVENTS AND HF JET ENERGY SCALE CALIBRATION AT 7 TEV IN THE CMS EXPERIMENT AT LHC

submitted by **BUĞRA BİLİN** in partial fulfillment of the requirements for the degree of **Master of Science in Physics Department, Middle East Technical University** by,

Prof. Dr. Canan Özgen _____
Dean, Graduate School of **Natural and Applied Sciences**

Prof. Dr. Sinan Bilikmen _____
Head of Department, **Physics**

Prof. Dr. Mehmet T. Zeyrek _____
Supervisor, **Physics Department**

Examining Committee Members:

Prof. Dr. Ali Ulvi Yılmazer
Physics Engineering Department, Ankara University _____

Prof. Dr. Mehmet T. Zeyrek
Physics Department, METU _____

Prof. Dr. Erhan O. İltan
Physics Department, METU _____

Prof. Dr. Altuğ Özpineci
Physics Department, METU _____

Prof. Dr. Müge Boz
Physics Engineering Department, Hacettepe University _____

Date: _____

I hereby declare that all information in this document has been obtained and presented in accordance with academic rules and ethical conduct. I also declare that, as required by these rules and conduct, I have fully cited and referenced all material and results that are not original to this work.

Name, Last Name: BUĞRA BİLİN

Signature :

ABSTRACT

PRODUCTION OF Z+JET EVENTS AND HF JET ENERGY SCALE CALIBRATION AT 7 TEV IN THE CMS EXPERIMENT AT LHC

Bilin, Buğra

M.Sc., Department of Physics

Supervisor : Prof. Dr. Mehmet T. Zeyrek

September 2011, 50 pages

Forward Jet Calibration for CMS detector is presented using Z boson + jet event samples in the pseudorapidity region of $0 < |\eta| < 5$. The results are based on proton-proton collision data at center of mass energy of $\sqrt{s} = 7$ TeV corresponding to $\sim$1 fb^{-1} of data. Z bosons are reconstructed from opposite sign lepton pairs ($\mu^+\mu^-$, e^+e^-) and the transverse momentum balance of the Z boson and the associated jet is used to derive the calibration coefficients. The coefficients are tested on jets from a WW Monte Carlo sample using the W-mass constraint. The W mass peak position is observed to be improved by $\sim$20 % without loss of resolution.

Keywords: Z+jets, Forward Jets, Calibration, LHC, CMS

ÖZ

LHC CMS DENEYİNDE 7 TEV'DE Z + JET OLAY ANALİZİ VE HF JET ENERJİ SKALA KALİBRASYONU

Bilin, Buğra
Yüksek Lisans, Fizik Bölümü
Tez Yöneticisi : Prof. Dr. Mehmet T. Zeyrek

Eylül 2011, 50 sayfa

CMS Detektöründe $0 < |\eta| < 5$ pseudorapidite aralığında, Z bozonu + jet olay numuneleri kullanılarak ileri jet kalibrasyonu gerçekleştirilmiştir. Sonuçlar $\sqrt{s} = 7$ TeV kütle merkezi enerjisindeki $\sim$1 fb $^{-1}$ lık proton proton çarpışma verilerinden elde edilmiştir. Z ayar bozonları zıt yüklü lepton çiftlerinden ($\mu^+\mu^-$, e^+e^-) geri oluşturulmuştur ve kalibrasyon katsayıları Z bozonu ile beraberindeki jetin dik momentum dengesi kullanılarak elde edilmiştir. Bu katsayılar W-kütle sınırlaması kullanılarak WW Monte Karlo numunesi üzerinde sınanmıştır. W kütle değerinin $\sim$ % 20 oranında geliştiği ve çözünürlük kaybı olmadığı gözlemlenmiştir.

Anahtar Kelimeler: Z+jet, İleri Jetler, Kalibrasyon, LHC, CMS

Işığıma, bana destek veren herkese.. Aileme ve dostlara....

ACKNOWLEDGMENTS

I would like to thank to the people whose helps were vital during hard working times on the thesis.

First of all, I would like to thank to my supervisor, Prof. Dr. Mehmet T. Zeyrek for his encouragement and patience throughout my studies. His encouragements triggered me to be in this field.

I would like to show my gratitude to Prof. Dr. Nural Akchurin and Dr. Efe Yazgan for their guidance throughout the work on the analysis and their kind support. Without their help and support, this thesis would not be possible. Also I am thankful to Keng Kovitanggoon (Texas Tech.) for his helps and friendship while working together.

Many thanks to my colleagues, Ilina Vasileva and Özgür Şahin for their endless help during the preparation of the thesis, and for helpful discussions on physics aspects and many technical details.

It is my pleasure to thank to my friends at CERN, Özlem Kaya and Eda Yıldırım for the good moments we shared between harsh working hours. The time we spent will always be in good memories of mine.

Special thanks to my dear love Göksu Koç for every single moment we shared, and for being with me in the most difficult times. Her love and friendship is and always will be invaluable for me.

Lastly, I am grateful to my family who grew me up and made me who I am. During tough moments in life, their endless support and love gave me the necessary motivation to fight with the difficulties. Without them, apart from thesis, life would not be possible.

TABLE OF CONTENTS

LIST OF TABLES

TABLES

LIST OF FIGURES

FIGURES

CHAPTER 1

INTRODUCTION

The Large Hadron Collider (LHC) machine at CERN is providing collisions since the end of 2009. Until August 2011, data corresponding to an integrated luminosity of $\sim$2 fb $^{-1}$ is collected by the CMS experiment.

CMS is one of the two multi-purpose detectors (ATLAS, CMS) for LHC. The two other major detectors at the LHC are ALICE and LHCb, where ALICE studies the aspects of heavy ion collisions, and LHCb focuses on b-physics. CMS focuses on a variety of physics topics at the TeV scale, such as verifying the Standard Model and searching new theories beyond the Standard Model.

The Standard Model of particle physics is the theory which explains the interactions of sub-atomic world. It is verified by the previous experiments and at the LHC experiments at a higher energy scale. Particles predicted by the Standard Model are observed except the Higgs boson, which might give mass to the elementary particles. One of the main goals of CMS experiment is to either prove or disprove the existence of the Higgs boson.

The jets, which are collection of charged and neutral particles, are originated from quarks (gluons) coming from the proton proton interactions. The jets then are reconstructed in the detector from the energy they deposit in the calorimeters. Due to detector effects, since the calorimeter response is not linear with respect to the initial energy, the measured jet energy is not equal to the originating quark (gluon), hence the jets need to be corrected accordingly.

Calibrating the forward jets plays an important role for detection and measurement of various physics processes. For one of the potential production channels of the Higgs boson, the Vector Boson Fusion process [1], the calibration of the forward calorimeter (HF) is important

for tagging jets involved in the process. The final state of VBF consist of the decay particles of the Higgs boson and two tagging jets whose distribution peaks at $|\eta| \sim 3$ and therefore a significant fraction of the jets lie in HF.

This thesis describes a method to calibrate the jets in the forward region of the CMS detector. There are various methods to calibrate jets at the CMS [2]. Some of them are at hardware level, which intend to correct the signals taken from the detector. Other methods aim to correct the overall scale of the jets. The method presented in this thesis is based on well balanced Z + 1 jet event samples from1.1 fb^{-1} portion of the p-p collision data collected by CMS detector in 2011. The transverse momentum ratio of the Z and the associated jet are used to calibrate the jets in the forward region. Previous studies in CMS using this method for calibrating jets in the central region can be found in [3]. The calibration study carried out in this thesis is summarized in the CMS Detector Note DN -2011/009 [4].

In Chapter 2, brief description of the theoretical aspects related to the analysis is presented. In Chapter 3, the basic principles of the LHC machine is presented. Also a brief description of the CMS detector, its structure and subsystems is given in this chapter. In Chapter 4, the Z + jet event selection criteria is explained. The analysis of Z + jet production is given in this chapter. In Chapter 5 the calibration work on forward calorimeter is presented. Jet energy scale corrections for the Hadronic Forward Calorimeter (HF) are derived by using well-balanced Z+jet events. These corrections can either be used at the detector level or as jet-energy scale corrections.

CHAPTER 2

STANDARD MODEL

In particle physics, the Standard Model [5, 6] refers to the theory describing the interactions of sub-atomic particles. The model covers the electromagnetic, weak, and strong interactions of the particles, where each force is mediated by one or more force-carrying bosons.

Elementary-particles of the Standard Model are either fermions with half integer spin, or bosons with integer spin. The fermions are grouped into leptons and quarks in three families. Figure 2.1 shows the table summarizing the basic properties of elementary particles.

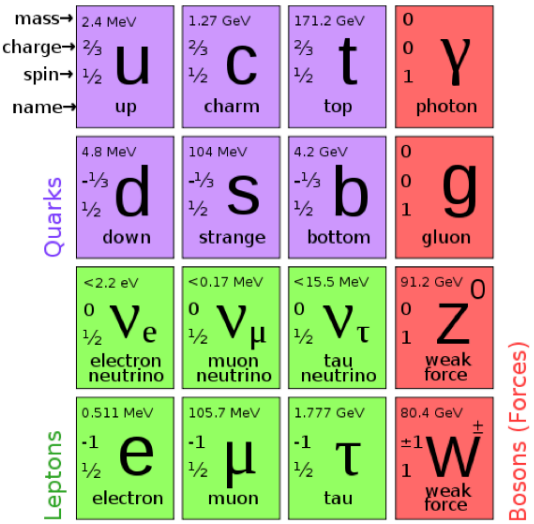

Figure 2.1: The Standard Model particles.

There are three families of fermions, and bosons are the mediators of forces. Photon is the mediating particle for Electromagnetic force, gluon is the mediator of the strong force, and

W and Z bosons are the carriers of the weak force. The photon and gluon are massless unlike the W and Z bosons. According to the theory, the quarks and gluons get combined to form hadrons. The hadrons are grouped into two, baryons and mesons. Baryons, like protons, neutrons, are made of three quarks of different colors. Mesons, like the pions, kaons, are made up of a quark and an anti-quark pair (There are possibly exotic hadrons or hadron molecules which does not necessarily consist of three quarks or quark anti-quark pair).

The Standard Model explains the interactions of fermions and bosons in terms of unitary groups as ;

$$SU(3)_{color} \otimes SU(2)_L \otimes U(1)_Y \tag{2.1}$$

Where $SU(3)_{color}$ symmetry of Quantum Chromodynamics (QCD) which represents the strong interactions of color-carrying quarks and gluons, and $SU(2)_L \otimes U(1)_Y$ represents the electro-weak interactions.

2.1 Electro-Weak Theory

It is the theory describing the electro-weak interactions of the sub-atomic particles, which combines the two forces of nature, the electromagnetic and the weak forces. It is mathematically represented by $SU(2)_L \otimes U(1)_Y$ symetry group.

The spontaneously broken $SU(2)_L \otimes U(1)_Y$ symmetry leads to the production of W and Z bosons. Before the spontaneous symmetry breaking, there are three W bosons rising from SU(2) (W^+ W^- W^0) and one boson from the U(1) (B_0). After symmetry breaking, the W^0 and B^0 mix and form the massive Z and the massless photon.

$$\begin{pmatrix} \gamma^0 \\ Z \end{pmatrix} = \begin{pmatrix} cos\theta_W & sin\theta_W \\ -sin\theta_W & cos\theta_W \end{pmatrix} \begin{pmatrix} B^0 \\ W^0 \end{pmatrix} \tag{2.2}$$

The W and Z bosons acquire mass after this breaking, whereas the photon remains massless. According to Particle Data Group book (PDG) [7], the Z mass is 91.1876 ± 0.0021 GeV, and the W mass is 80.398 ± 0.025 GeV.

2.2 Quantum Chromo Dynamics (QCD)

QCD is a theory [6] which explains the interactions of color-charge (red-green-blue) carrying quarks and gluons; the strong interactions. QCD is based on $SU(3)_{color}$ symmetry and has 8-generators, which leads to eight types of gluons, which carry color-charge in order to conserve the color charge in strong interactions. Since the gluons themselves carry color-charge, they can interact with themselves strongly. The leptons, not carrying color-charge, does not interact strongly.

When quarks move away from each other, the potential energy of the system increases. Once enough energy is stored, a quark- antiquark pair is created and reduces the potential energy. This lead to the hadronization; as the quark (gluon) produced moves with high speed, it fragments and forms mesons and baryons. This fragmentation leads to the production of jets, a group of hadrons bursted in the direction of the originating quark (gluon). Figure 2.2 shows a schematic view of fragmentation which leads to hadronization.

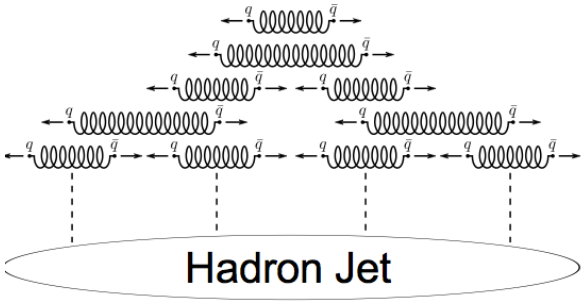

Figure 2.2: Fragmentation of quarks moving away from each other, and forming jets of particles.

The jets originated from the quark or gluon from the interaction consists of many charged and neutral particles; mesons, baryons and the photons due to Electromagnetic interactions of the charged particles. The jets, consisting of these particles leaves some of their energies in different parts of the detector. The charged fraction of the jets leaves traces at the tracker, the hadronic particles on the jet leave some of their energy in Hadronic Calorimeter, from which the jet energy is reconstructed. The Hadronic Calorimeter measures the energy of the jet with resolution less than one, so the measured jet energy needs to be corrected with respect to the originating parton.

2.3 Z + Jet Production

The leading order process for the Z production at LHC is the Drell-Yan process, in which a quark and anti-quark from the colliding baryons combine to form the Z boson. The Feynman diagram for the leading order Z/γ^* production is shown in Figure 2.3.

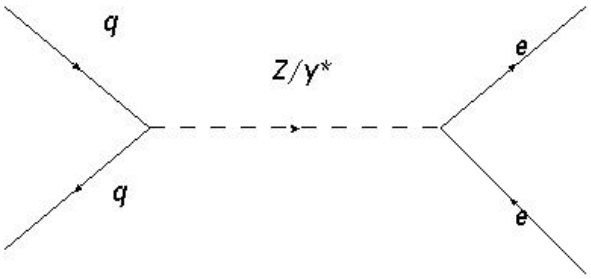

Figure 2.3: Drell Yan process for Z/γ^* production at hadron colliders.

In higher order processes, Z is accompanied by either a gluon or a quark, which then forms the jets. Some of the Feynman diagrams for the Z + N jet processes are shown in Figure 2.4.

The Z boson, after being produced decays into a pair of fermions. The decay width of Z boson to the different types of fermions are dependent on the mass of the fermions. Due to the high mass of the top quark, the number of decay channels of Z boson reduces to 11, 6 lepton and 5 quark channels. The decay width of the Z boson is dependent on the decay channel. The partial decay width of the Z boson into a pair of leptons is given in the formula.

$$\Gamma(Z \to ll) = \frac{G_F\, M_Z^3}{6\ \sqrt{2}} \left(|g_A^l|^2 + (|g_V^l|^2\right) \tag{2.3}$$

According to Particle Data Group book (PDG) [7] the branching ratio of Z decaying hadronically is 69.91 ± 0.06%. The BR of Z(ee) is 3.363 ± 0.004% and of Z($\mu\mu$) is 3.366 ± 0.007%.

The leading order Z production with no associated jets has low transverse momentum due to the fact that all the initial transverse momenta of the initial partons are carried by the Z boson. For the Z + jet processes the Z transverse momentum is balanced by the accompanying jets. This effect can be directly observed in the Z transverse momentum distributions. The Z + N jet measurements can be used for testing the perturbative QCD predictions.

The measurement of Z + jet production also serves as background for many Standard Model

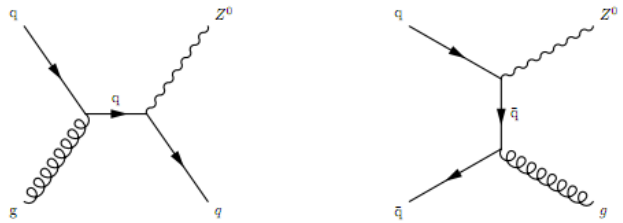

(a) Z + 1 jet

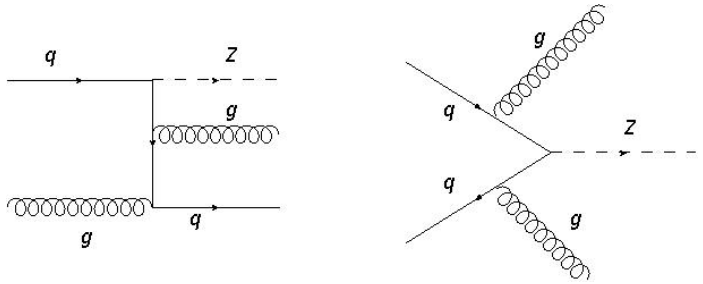

(b) Z + 2 jets

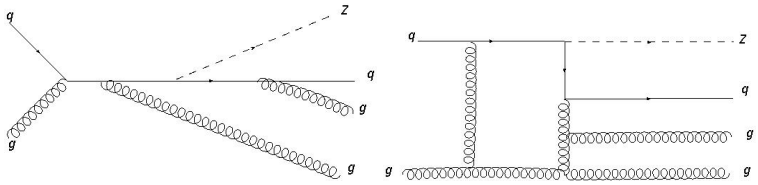

(c) Z + 3 jets

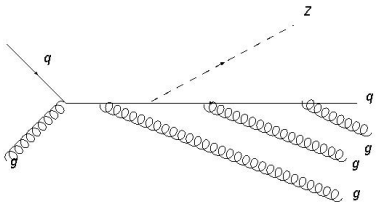

(d) Z + 4 jets

Figure 2.4: Feynman diagram's of next to leading order Z+jet productions.

processes, and also for the searches of Beyond Standard Model particles, which are supposed to decay to jets and charged leptons. Hence, Z + jet production process is a base analysis for the precise measurement of the Standard Model events and for new physics studies.

CHAPTER 3

LHC AND CMS

3.1 The LHC Machine

The Large Hadron Collider (LHC) [8], being the world's largest hadron collider, is now in operation since the end of 2009. LHC is mainly a proton-proton collider, colliding protons at a center of mass energy of 7 TeV but the design collision energy is 14 TeV. It also serves as a lead ion collider, typically one month per year.

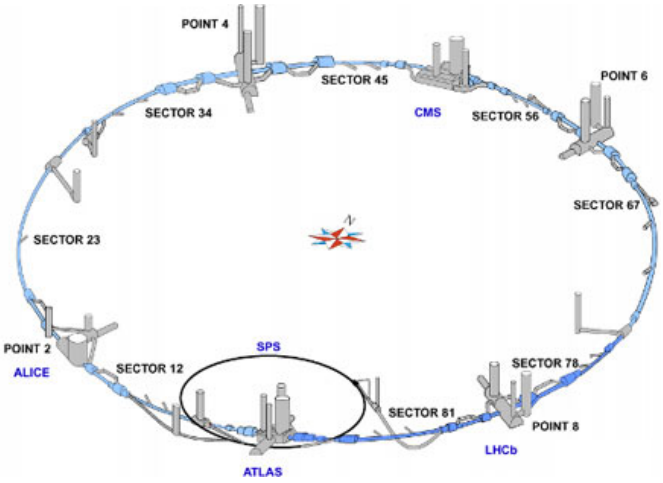

Figure 3.1: The Layout of LHC and the experiments [9].

LHC is built in a tunnel of 27 km circumference near Geneva Switzerland and extends to France, lying underground at a depth between 50-175 m. There are four major experiments based at the LHC; ALICE, ATLAS, CMS and LHCb. Among those, two large experiments; ATLAS and CMS are general-purpose detectors focusing on wide range of physics topics. The other experiments, ALICE and LHCb are specialized detectors focusing on heavy ion

and b-physics respectively. There are also smaller detectors like LHCf and TOTEM focusing on forward physics. Figure 3.1 shows the layout of the LHC and the experiments.

The protons (ions) are accelerated in multiple steps. Before being injected into the LHC tunnel, the protons gains energy in the Linear Accelerator (LINAC), Proton Synchrotron (PS) and Super Proton Synchrotron (SPS) in the listed order and then they enter the LHC with an energy of 450 GeV per beam. Then the protons are accelerated to 3.5 TeV of energy per beam. The first stage of heavy ion acceleration is done in LINAC3 and then they enter the Low Energy Ion Ring (LEIR). Then they enter the PS and follow the same way as protons. Figure 3.2 shows the sequence of proton/ heavy ion acceleration up to LHC.

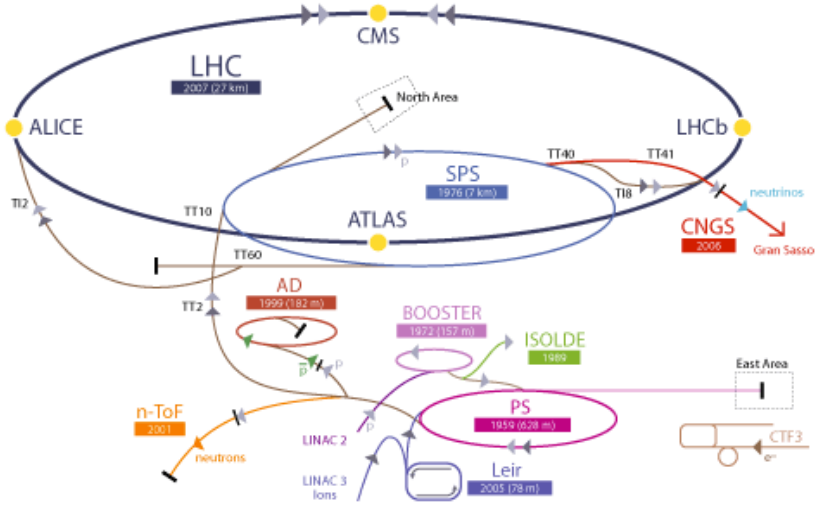

Figure 3.2: The sequence of acceleration for protons and lead ions [9].

LHC has ~1600 superconducting magnets installed, where the dipole magnets aim to bend the track of the proton beams, and the quadruple magnets squeeze the beam to get more collisions from each crossing proton bunches. The magnets operate at a temperature of 1.9 K, and the operation temperature is maintained by liquid helium.

3.2 The CMS Detector

The Compact Muon Solenoid [10] is a general-purpose detector built to detect particles produced by the LHC collisions. It is built at the experimental cavern at P-5 of the LHC, situated near Cessy, France. General layout of the experiment is shown in Figure 3.3.

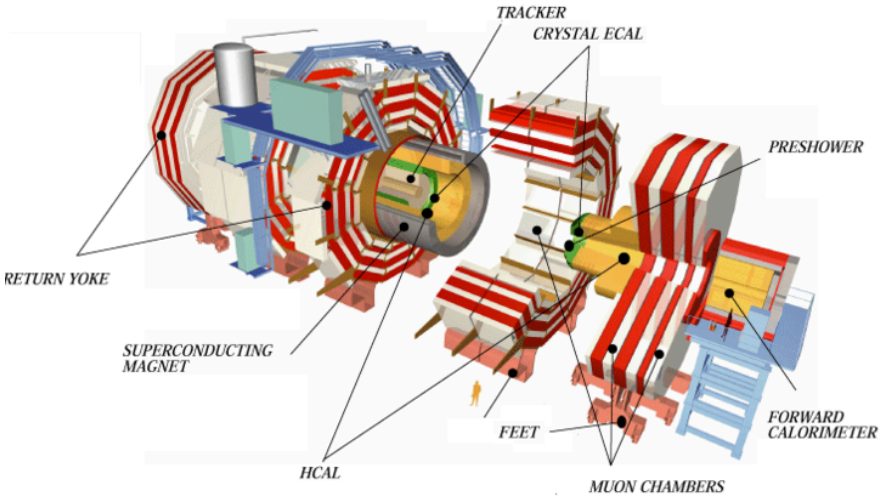

Figure 3.3: General Layout of the CMS experiment [12].

Some of the aims of the CMS experiment can be listed as;

- To explore physics at the TeV scale.
- To understand the source of electroweak symmetry breaking.
- To study aspects of heavy ion physics.

CMS, like its predecessors, consists of many sub-detectors built like an "onion" as layers in sequence, each of which aims to measure the properties of different particles coming from the interactions. The transverse view of the CMS detector showing the different sub-detectors is shown in Figure 3.4. This figure illustrates paths and showers of different types of particles.

3.2.1 The Magnet

The magnet of the CMS detector [17] is a superconductor solenoid magnet of 6 m of diameter, which provides 3.8 T of magnetic field. The current needed for 3.8 T of field is 18,160 A, which gives a stored energy of 2.3 GJ. The magnetic field is important for measuring the charge/mass ratio and the momentum of the charged particles since the magnetic field bends the charged particle tracks.

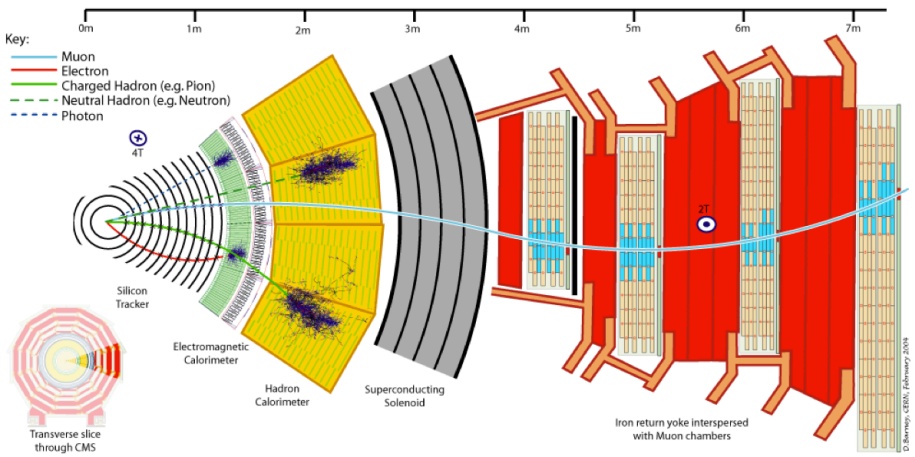

Figure 3.4: Transverse View of the CMS detector [12].

3.2.2 Tracking System

The tracking system of the CMS detector [13] aims to measure the momentum and trajectory of the charged particles. It is made up of 1440 pixel and 15148 strip detector modules. The reconstruction of the tracks of leptons and hadrons can be carried out in a rapidity range of $|\eta| < 2.5$. As the charged particle propagates through the tracking material, it creates electric signals which are then amplified and detected. The track of the charged particles are reconstructed from the "hits" they create on different layers of the Tracker. The momentum of the particle is found from the bending of the particle track in 3.8 T magnetic field. The CMS tracker includes inner trackers at which the density of tracks is the highest. The inner tracker is made of silicon pixel detectors, in a rapidity range of $|\eta| < 2.5$, and measures the tracks with a resolution of 15 μm. Silicon strip detectors with lower track intensities surround the pixel detectors.

3.2.3 Calorimeters

The electromagnetic and hadron calorimeters form a complete calorimetry system, which is essential for the measurement of jets and missing transverse energy. The calorimeters are briefly described below.

3.2.3.1 Electromagnetic Calorimeter

The Electromagnetic Calorimeter (ECAL) [14] surrounds the Tracker, which aims to measure the energies of the photons and the electrons. It covers the rapidity region of $|\eta|$ <3.0 and has two parts, the Barrel (EB) and the Endcap (EE); both in the solenoid magnet volume. EB covers the central region of $|\eta|$ <1.479 and consists of 61200 lead tungstate (PbWO4) crystals. EE covers the region of 1.479< $|\eta|$ <3 and has 7324 crystals on each side. One quadrant of the Calorimeters is shown in Figure 3.5.

ECAL measures the amount of energy that the particles leave in the crystals. When the particles propagate through the crystals, they leave some portion of their energy by scintillation. The scintillation light produced is then detected by photodetectors and converted to electronic signals, and to energy.

Preshower

The Preshower (ES) is made of two thin lead converters which lies in front of EE in pseudo-rapidity region of 1.653< $|\eta|$ <2.6 as seen in Figure 3.4. The aim of the ES is to distinguish single high-energy photons from close pair of low-energy photons. It has a total thickness of 20 cm.

3.2.3.2 Hadron Calorimeter

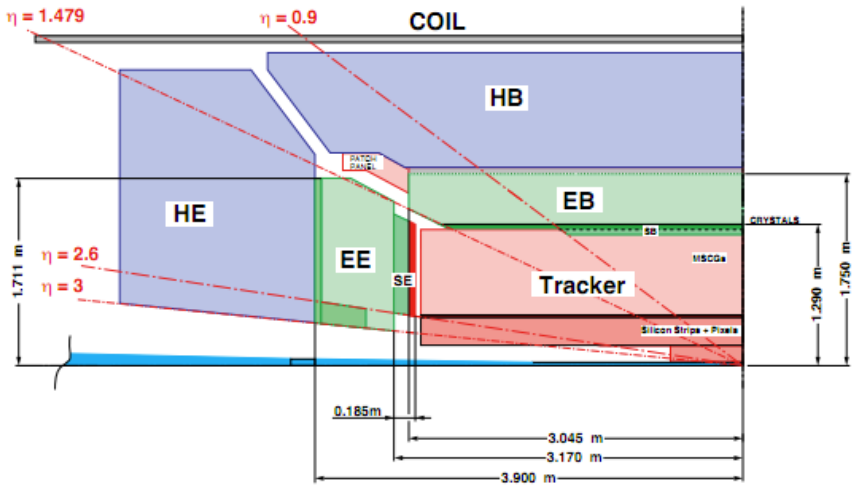

Figure 3.5: Schematic view of one quadrant of the calorimetry and tracking system [14].

The next layer of the CMS detector after ECAL is the Hadron Calorimeter (HCAL) [15] which measures the energy of jets. It consists of central calorimeters (Barrel and Endcap) lying inside the solenoid magnet covering the rapidity range $|\eta|$ <3, and forward calorimeter outside the magnet.

HCAL Barrel (HB) and HCAL Endcap (HE) Calorimeters

The central hadron calorimeter consists of active material of 4mm thick plastic scintillator tiles; and absorber plates of thickness of 5 cm in HB and 8 cm in HE which are made up of copper. A hadron interacts with the absorbers and creates showers of particles which create scintillation in the scintillator tiles. Then the amount of scintillation is combined and converted to the particles energy.

HCAL Forward Calorimeter (HF)

The Forward Calorimeter (HF) [16] covers a range of 2.853< $|\eta|$ <5.191. Unlike the central HCAL, HF has absorber plates that are made up of steel and the active material is made of quartz fibers due to harsh radiation conditions in the forward region.

The HF consists of the absorber structure that is composed of 5 mm thick grooved plates. The quartz fibers are inserted into these grooves. There are two types of fibers, which are independently measured, with different lengths, named *long* and *short* fibers. The long fibers run through the whole absorber material of 165 cm in depth. The short fibers edges are behind 22 cm of steel. This is important to identify the showers generated by electrons and photons, which deposits its energy mostly on the long fibers since for most of the cases they can not reach the short fibers behind 22 cm of steel material. On the contrary, the showers generated by hadrons create signals in both of the fibers. The structure of HF is shown in Figure 3.6.

HF consists of 13 η rings on each side. Table 3.1 shows the index and the corresponding η range for HF towers.

3.2.4 The Muon System

The muon system of the CMS detector [18] aims to identify the muons precisely. The muon system consists of three different kinds of detectors; Drift Tubes (DT), Cathode Strip Chambers (CSC), and Resistive Plate Chambers (RPC).

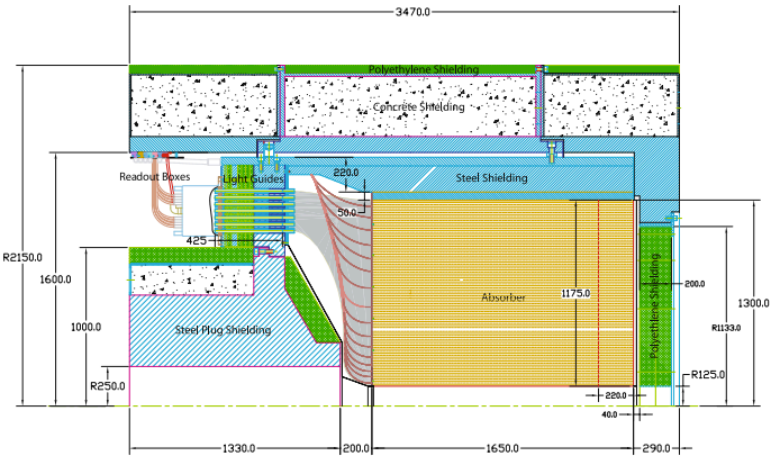

Figure 3.6: The HF Calorimeter [16].

Table 3.1: HF rapidity ranges and corresponding azimuthal angle size.

tower index	η range	Size in ϕ
29	2.853-2.964	10°
30	2.964-3.139	10°
31	3.139-3.314	10°
32	3.314-3.489	10°
33	3.489-3.664	10°
34	3.664-3.839	10°
35	3.839-4.013	10°
36	4.013-4.191	10°
37	4.191-4.363	10°
38	4.363-4.538	10°
39	4.538-4.716	10°
40	4.716-4.889	20°
41	4.889-5.191	20°

DT's are located at the central barrel region ($|\eta|$ <1.2) and the CSC's are at the endcap region (1.2< $|\eta|$ <2.4). The RPC's are located at both barrel and endcap, and they have much faster response than the DT's and CSC's, hence are used for triggering, whereas the former ones measure the position of muons precisely. Layout of the CMS Muon system is shown in Figure 3.7.

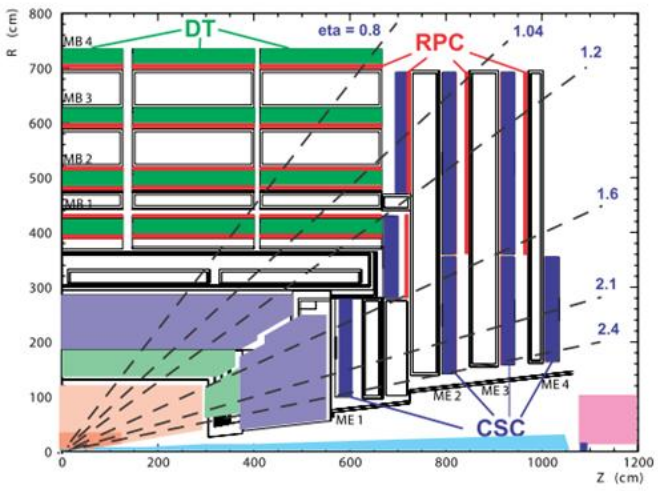

Figure 3.7: CMS Muon system showing the layout of RPC's, DT's and the CSC's [18].

3.2.5 Monte Carlo Event Generation and Detector Simulation in CMS

The simulation of events in the CMS experiment is based on Monte Carlo techniques and carried out in steps by different MC Generators. Firstly, the generation of the proton proton collisions and particle level hard scattering processes are carried out. The generation step can be carried out by Matrix Element generators such as Alpgen, Madgraph, Powheg [19], which also implements NLO calculations, or by Pythia. Then, the output of the ME generators is given to Pythia [20] for hadronization step of the generated particles through the CMS Software Framework.

After generating the Monte Carlo events, the simulation of the CMS detector is carried out using GEANT-4 program [21]. The detector simulation of events which are generated in the previous step is carried out, as it would happen in a real experiment. Then, the standard reconstruction step regarding the digitization of detector hits as simulated by the generated particles and the reconstruction of physical objects from the simulated detector information is followed to obtain datasets similar to the ones gathered from real collision data.

3.2.6 CMS Trigger and Data Acquisition

The main goal of the trigger and data acquisition systems [22] is to provide fast decisions on the good events to be stored out of $\sim 10^9$ interactions occurring every second. The input

rate should be reduced to order of few 100 events per second. The CMS trigger system was designed to achieve this in 2 steps. All of the collected data is firstly kept for 3.2 μs before being triggered, and then the 100 kHz portion of all events is forwarded to the High Level Trigger algorithms. The CMS event selection procedure starting from the detector signals is illustrated in Figure 3.8.

There are two levels of triggers, one of which, the Level-1 is purely hardware based, using information from calorimeter and the muon system information, and the high level trigger(HLT) relies on processors with some trigger algorithms. The trigger and Data Acquisition system (DAQ) should be fast enough to decide in 3.2 μs which portion of the data is useful to be stored and copy that data from the front-end pipelines, where the data from detector is stored for that amount of time. According to the physics needs, different sets of triggers provides different datasets. For the Z+jet analysis , we used the events from double-lepton triggered datasets.

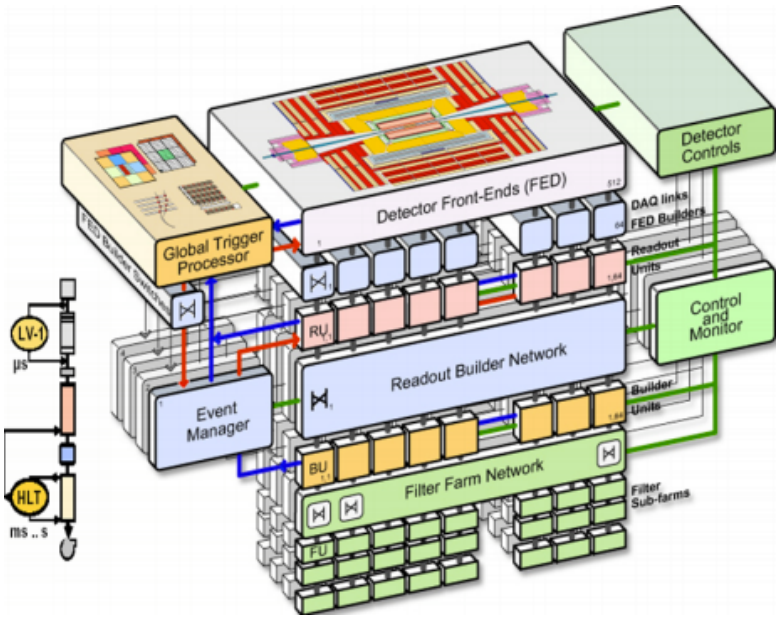

Figure 3.8: CMS Event Selection [23].

3.2.6.1 L1 Trigger

The L1 triggers use information from the calorimeters and the muon system, based on the identification of muons, electrons, photons, jets, and missing transverse energy. The trigger

system is based on the L1 calorimeter and the L1 muon triggers which builds the L1 global trigger. The tracker information can not be used at this level of triggering due to the size of their data. The calorimeter trigger relies on the reconstructed-hits (rec-hits) of HCAL and ECAL, where the muon trigger uses information of the three muon systems, the RPC's, the CSC's and the DT's. After deciding which event is to be taken or not after L1 triggering, the decision is passed to the front ends via the Trigger Timing and Control system(TTC). The Figure 3.9 shows the steps of L1 Trigger.

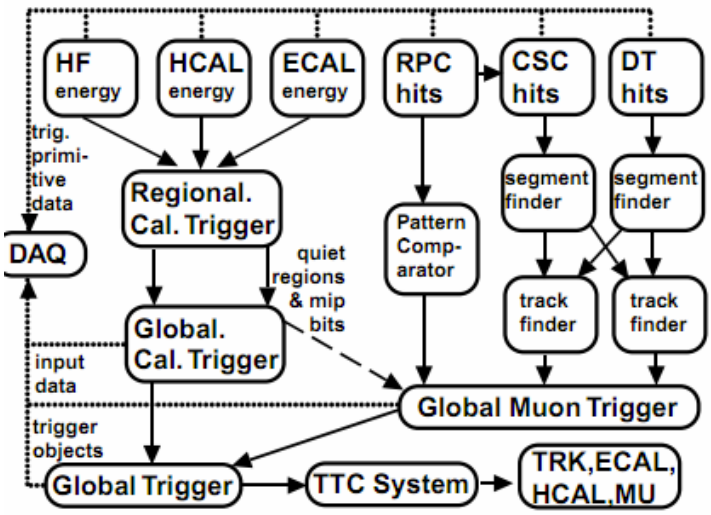

Figure 3.9: L1 trigger schema [23].

3.2.6.2 High Level Trigger

CMS High Level Trigger (HLT) relies on trigger algorithms. For optimal flow of data, event selection is performed in multiple stages by appliying High Level Trigger filters. The HLT farm can reach the L1 information and some extra that were not used in L1 step, such as tracker information and principally all the data with full granularity.

3.2.7 CMS Software Framework

CMS Software Framework (CMSSW) is the main software regarding all the steps from data taking to the analysis level. It is a modular software based on mainly C++ and python. The schematic view of the modular software is shown in Figure 3.10.

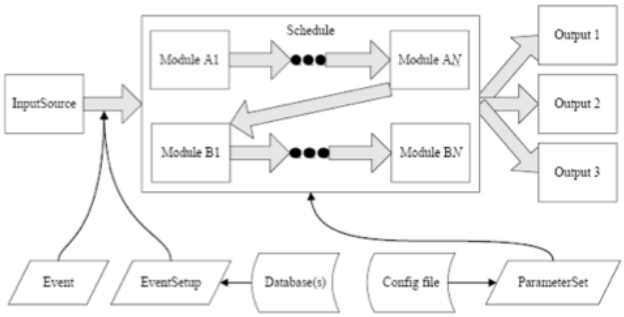

Figure 3.10: CMSSW framework.

It is based on Event Data Model (EDM) framework, running with a single executable. The events are stored under a singe entity in memory; edm::Event vector. The CMSSW modules can be summarized as EDProducer, EDAnalyzer, EDFilter, EDLooper etc.

3.2.7.1 Event Data Model

Event Data Model (EDM) [24] forms the basic format for storing and analyzing the data. In this concept, an event is defined to be a collection of C++ classes, containing each bit of data of different physical objects such as reconstructed electrons, muons, jets; collections of trigger and signals from different sub-detectors, such as tracker collection, calorimeter rec-hits. etc. All the data and the physical objects are identified from the "signals" they leave in the detector. The physical objects are reconstructed from the detector information through different steps of reconstruction using CMSSW framework. The same procedure is followed for both simulation and the real data collected from collisions.

The event information starting from the detector response to the reconstruction of the physical observables are collected in so called data-tiers. The main data-tiers regarding the flow of data of CMS can be summarized as RAW, DIGI, RECO and AOD for real data and GEN, SIM, DIGI for the MC simulation. The content of different data tiers is illustrated in Figure 3.11.

- RAW contains all detector data and the trigger information. The object reconstruction is based on the RAW data.
- DIGI is made up of the raw data collected by the detector which is converted to digital

signals.

- RECO consists of all objects from reconstruction step, based on the RAW data. It contains reconstructed physics objects for analysis purposes.
- AOD is a data-tier based on RECO data to provide data for analysis purposes. The AOD files contain less objects than the RECO tier, which is sufficient for most of the physics analysis.
- GEN contains information of the generated Monte Carlo event before the detector simulation step.
- SIM contains the energy depositions of detector simulation results for the generated level particles.
- DIGI (MC) is the converted version of SIM information to the detector response, with the same structure of RAW data. The reconstruction of MC events follow the same procedure as the data based on DIGI events.

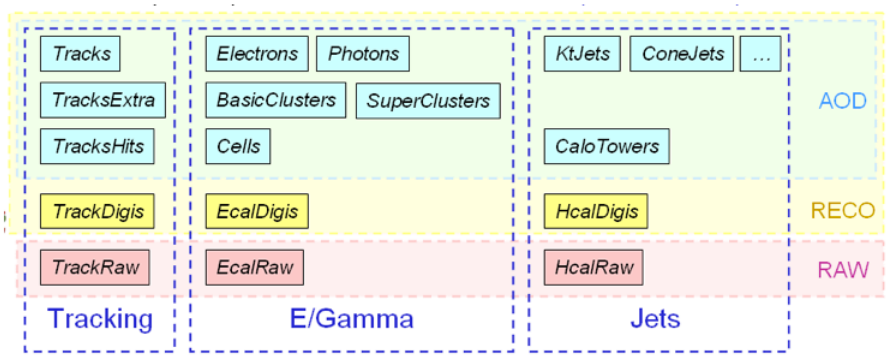

Figure 3.11: Content of different Data Tier files for some objects [24].

The event data files are stored in ROOT [25] file format. The high level physics objects are kept in collections depending on their type. The physical objects are kept under the Candidate collection, and each collection of objects (electrons, muons) have reference to the related objects (Tracker, Calorimeter, Muon system information).

CHAPTER 4

Z+JET PROCESS

4.1 Event Reconstruction and Selection

The analysis presented in this thesis is based on the reconstruction of Z + jet processes. In this chapter, the selection procedure of the Z + jet events is briefly described. The sets of data, reconstruction of physical objects and the selection variables related to the procedure of selecting Z + jet events are given.

4.1.1 Samples

The data samples used for the analysis is given in this section. There are two main sets of samples, one of them is the data samples from real proton-proton collisions collected by CMS experiment, and the other one is based on the event generation and the simulation of the CMS detector using Monte-Carlo techniques, namely Monte-Carlo samples.

4.1.1.1 Data Samples

For the analysis, datasets with mainly double-lepton triggered events are used. The "good" portion of the recorded data is used for which all sub-systems are required to function properly for each portion of data; lumi section. The list of datasets used in this analysis is shown in Table 4.1. The corresponding "Json" files which are utilized to select the good portion of the data are displayed in Table 4.2.

Table 4.1: Datasets of 2011 data and corresponding run numbers.

/DoubleElectron/Run2011A-May10ReReco-v1/AOD	160431 – 163869
/DoubleElectron/Run2011A-May10ReReco-v1/AOD	165088 – 167913
/DoubleMuon/Run2011A-PromtReco-v4/AOD	160431 – 163869
/DoubleMuon/Run2011A-May10ReReco-v1/AOD	165088 – 167913

Table 4.2: Json files corresponding to the 2011 dataset to choose good portion of data.

Cert_160404-163869_7TeV_May10ReReco_Collisions11_JSON_v2.txt
Cert_160404-167913_7TeV_PromptReco_Collisions11_JSON.txt

4.1.1.2 Monte Carlo Samples

Monte Carlo Samples for signal and various backgrounds used for the analysis is summarized in Table 4.3.

Table 4.3: Monte Carlo Samples (*Summer11-PU_S4_START42_V11-v1/AODSIM).

/DYToEE_M-20_CT10_TuneZ2_7TeV-powheg-pythia/*
/DYToMuMu_M-20_CT10_TuneZ2_7TeV-powheg-pythia/*
/DYToTauTau_M-20_CT10_TuneZ2_7TeV-powheg-pythia/*
/WplusToENu_M-20_CT10_TuneZ2_7TeV-powheg-pythia/*
/TT_TuneZ2_7TeV-powheg-pythia/*
/WW_TuneZ2_7TeV_pythia6_tauola/*
/WZ_TuneZ2_7TeV_pythia6_tauola/*
/ZZ_TuneZ2_7TeV_pythia6_tauola/*

In the Monte-Carlo sample names; the CT10 [26] stands for the parton distribution function for simulating the distribution of quarks and gluons in the protons, Tune Z2 is the fine tuning setting of Pythia [20] for simulating the interactions at the LHC conditions. M-20 stands for the production level mass cut (M > 20 GeV) for the generated particle.

For overlaying the distributions, the Monte-Carlo samples for the Z signal and backgrounds are normalized to the total integrated luminosity of the data.

$$N = \sigma \times \int Ldt \times \epsilon \tag{4.1}$$

Where σ stands for the generator-level cross section of the process, $\int Ldt$ is the total integrated luminosity and the ϵ stands for the efficiency regarding reconstruction, isolation, identification and trigger efficiencies. The processes regarding Z boson signal and some backgrounds, and the corresponding cross sections are summarized in Table 4.4 for an integrated luminosity of 1.132 fb^{-1}.

Table 4.4: Cross Sections and the expected number of events in 1.132 fb^{-1} data for various processes.

Process	x-sec(pb)	ϵ^{filter}	ϵ^{cut} (%)	N^{exp}
$Z/\gamma^* \rightarrow ee$	1666	1	11	214243
$Z/\gamma^* \rightarrow \tau\tau$	1666	1	0.031	585
$W^+ \rightarrow e^+ \nu_e$	5404.0	1	0.002	122
$t\bar{t}$	157.5	1	0.43	767
ZZ	4.287	1	2.04	99
WZ	10.47	1	1.04	123
WW	27.83	1	0.37	117

4.1.2 Lepton Reconstruction

Electrons

Electrons in CMS [27, 28] are reconstructed from the information gathered from the Tracker and the Electromagnetic Calorimeter. To measure the energy of an electron, the amount of the tracker material in front of the calorimeter is taken into account. When traversing through the silicon layers, electrons radiate photons via bremsstrahlung process. The energy reaching the ECAL will spread in the azimuthal direction due to the magnetic fileld. The ϕ spread and the amount of bremsstrahlung energy is taken into account by the ECAL clustering. Supercluster-driven pixel-seed finding is then used to initiate the building of trajectories in the inner tracker. Track reconstruction of electrons is based on a "Gaussian sum filter" using a specific energy loss modeling.

After reconstructing electrons from detector signals, the isolation and selection variables are applied. Electrons are selected from the central region ($|\eta| < 2.5$) except a pseudorapidity gap between ECAL Barrel and Endcap transition region ($1.4442 < |\eta| < 1.560$). Electron candidates are required to have transverse momentum (P_T) larger than 20 GeV. Electron identification and isolation criteria described below are applied. For the analysis two different cut-sets

for electron selection are used. One of them, WP80 (Working Point 80) which selects electrons with 80 % is used for this chapter in order to get cleaner Z samples. With this cut-set, the number of Z + jet events in $\sim$ 1 fb^{-1} of data are not sufficient to carry out the calibration of forward calorimeter, hence for the calibration purpose, a looser cut set of WP95 to select electrons with 95% efficiency is used. Once more data will be collected by the CMS experiment, the tighter cut-set can be chosen. The cuts and the values are summarized in Table 4.5.

- $H/E \rightarrow$ Ratio of the energy in HCAL to the super-cluster energy of the electron candidate.

- $I_{ECAL} \rightarrow$ The sum of the transverse energy (E_T) of the ECAL RecHits in a cone size of $\Delta R < 0.3$ arround the electron, normalized by dividing to the (E_T) of the electron candidate.

- $I_{HCAL} \rightarrow$ The sum of transverse energy (E_T) form the HCAL towers in a cone size of $\Delta R < 0.3$ arround the electron, normalized by dividing to the (E_T) of the electron candidate.

- $I_{Tracker} \rightarrow$ The sum of the Transverse Energy (E_T) of the tracks in a cone size of $\Delta R < 0.3$ arround the electron, normalized by dividing to the (E_T) of the electron candidate.

- $\Delta\eta \rightarrow$The pseudorapidity difference of the supercluster center of the electron candidate and the associated track at the vertex.

- $\Delta\phi \rightarrow$The ϕ angle difference of the supercluster center of the electron candidate and the associated track at the vertex.

- $\sigma_{i\eta i\eta} \rightarrow$ The shower-shape variable (rapidity-width) of the supercluster in unit of crystal, where 5 x 5 crystals around the seed is taken into account.

- missing hits$\rightarrow$ The number of tracker layers not receiving a hit by the electron from the interaction point.

- $d_0 \rightarrow$ The distance between the track of the electron and the closest track.

Table 4.5: Electron cut-sets for WP80 and WP95.

Paremeter	WP80		WP95	
	Barrel	Endcap	Barrel	Endcap
H/E	< 0.025	< 0.04	< 0.01	< 0.03
I_{ECAL}	< 0.05	< 0.07	< 2.0	< 0.06
I_{HCAL}	< 0.025	< 0.10	< 0.12	< 0.05
$I_{Tracker}$	< 0.04	< 0.09	< 0.15	< 0.08
$\Delta\eta$	< 0.007	< 0.004	< 0.007	–
$\Delta\phi$	< 0.03	< 0.06	–	–
$\sigma_{i\eta i\eta}$	< 0.03	< 0.01	< 0.01	< 0.03
missing hits	$= 0$	$= 0$	≤ 1	≤ 1
d_0	> 0.02	> 0.02	–	–

The transverse momenta distribution of leading electrons is shown in Figure 4.1 and the rapidity distribution is shown in Figure 4.2.

Muons

The muons in CMS detector [29] are reconstructed from the information gathered from the muon detectors and the tracker. Firstly the muon hit information are combined as segments. Then these segments from different muon detectors combine to form the Muon Seeds. Finally the combined seeds are matched with the inner tracker information for the reconstruction of the global muons. Different muon algorithms rely on different steps of the muon reconstruction. In the analysis the muons of both Global and Tracker Muon algorithms are used. The selection variables described briefly below are used to identify muons. The cut-set is summarized in Table 4.6.

- $\Sigma P_T(\Delta R = 0.3) \rightarrow$ Sum of Transverse momenta in a cone size of 0.3 around the muon candidate.
- $|d_{xy,muon}| \rightarrow$ Impact parameter in the transverse (x,y) plane which is calculated with respect to the beam spot.
- Number of pixel hits$\rightarrow$ Number of hits the muon creates on the pixel detectors.
- Number of tracker hits$\rightarrow$Number of hits the muon creates on the silicon trackers.
- Number of valid Muon hits$\rightarrow$Number of hits the muon creates in the muon system.

- $\bar{\chi^2}$ of the global fit→ Is the fit parameter between the muon detector and the tracker information regarding the reconstruction of global muons.

Table 4.6: Muon cut-sets.

Paremeter	Value
$\Sigma P_T(\Delta R = 0.3)$	< 3 GeV
$\lvert d_{xy,muon} \rvert$	< 0.2 cm
Number of pixel hits	> 1
Number of tracker hits	> 1
Number of valid Muon hits	≥ 1
$\bar{\chi^2}$ of the global fit	< 10

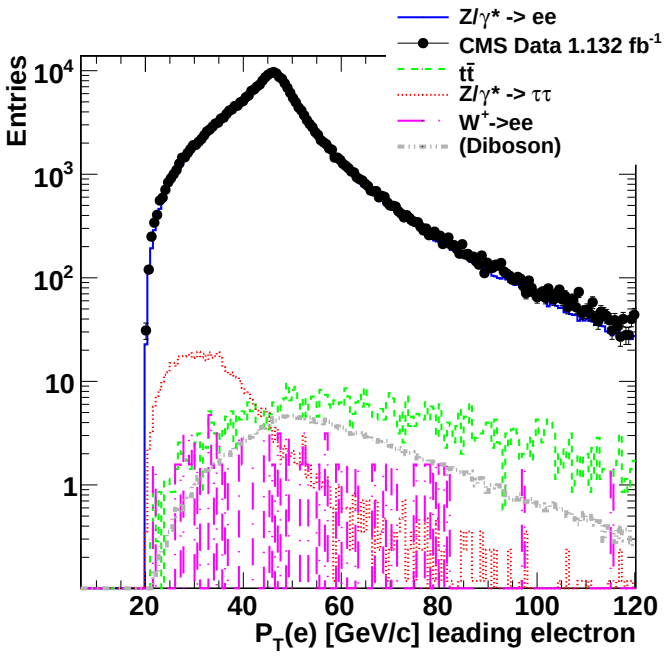

Figure 4.1: Transverse Momentum (P_T) distribution of leading electrons.

4.1.2.1 Di-Leptons

Di-leptons are reconstructed by the two leptons with highest transverse momentum (P_T) passing the selection & identification variables as described in detail in the previous section. The events having di-electron mass between 60 GeV and 120 GeV are accepted. No further cuts

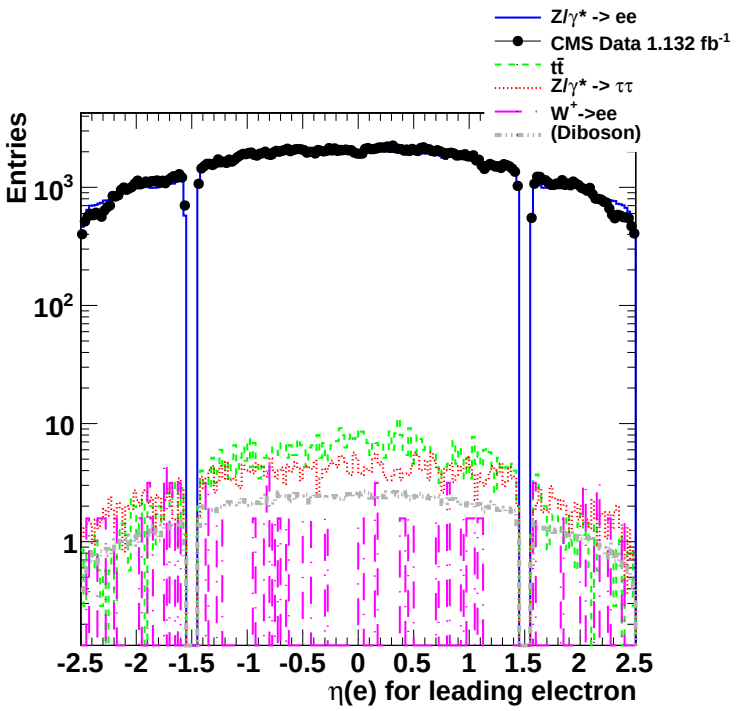

Figure 4.2: Pseudorapidity (η) distribution of leading electrons.

are applied on the Z-candidate variables. The Z mass distribution from di-electrons is shown in Figure 4.3, Figure 4.4 shows the rapidity distribution, and Figure 4.5 shows the azimuthal angle distributions of Z boson candidates.

4.1.3 Jets

Anti-kt jet algoritm [30] is used with a cone size of $\Delta R < 0.5$, where $\Delta R = \sqrt{(\Delta\eta)^2 + (\Delta\phi)^2}$. The jets used are the Calo-Jets, reconstructed using Calorimeter hits information. Jets are required to have minimum distance ΔR of 0.5 to the electrons which form the Z-candidates.

The reconstructed jets are required to have minimum transverse momentum of 30 GeV and no restrictions are applied on the pseudo-rapidity of the jets .Transverse momentum distribution of the leading jets accompanying the Z candidates in the mass window is shown in Figure 4.6.

Number of jets in Forward region accompanying Z candidates within the mass window is shown in Figure 4.7.

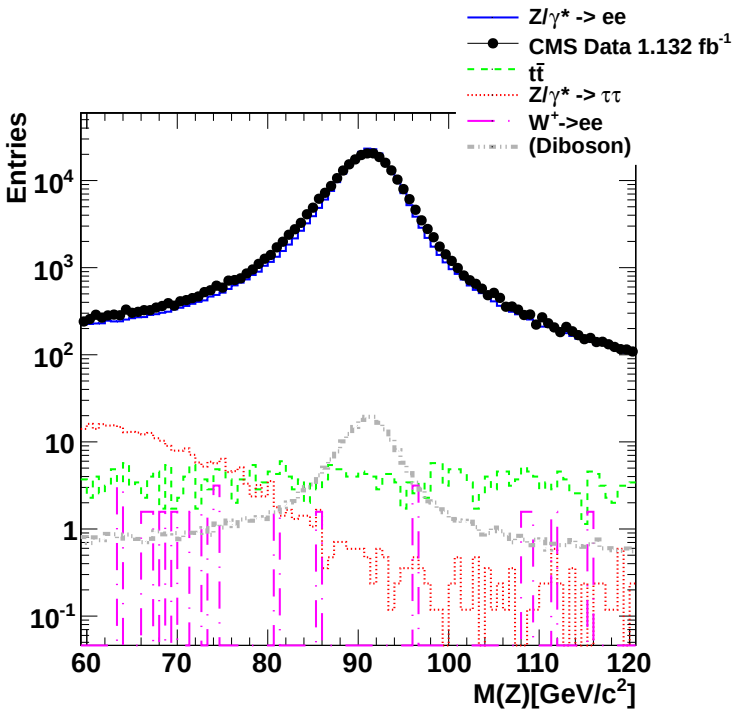

Figure 4.3: Z mass reconstructed from di-electrons.

4.2 Z + Jet Events

In this section, kinematical observables of Z + jet events passing the selection procedure is given. The physical variables of the Z boson candidates and the jets accompanying them are presented.

The Z mass and the transverse momentum are shown for the Z + 1 jet events; Figure 4.8 shows the Z mass and Figure 4.9 the P_T for the Z reconstructed from electrons. Figure 4.10 shows the Mass and Figure 4.11 shows P_T distribution for the Z + jet events with the jet in HF.

From the distributions it can be seen that the data points are in good agreement with the Monte Carlo simulation, and the background effects from various processes is seen to be small. Due to small background involved, this process provides a clean sample to be used for calibrating jets in HF.

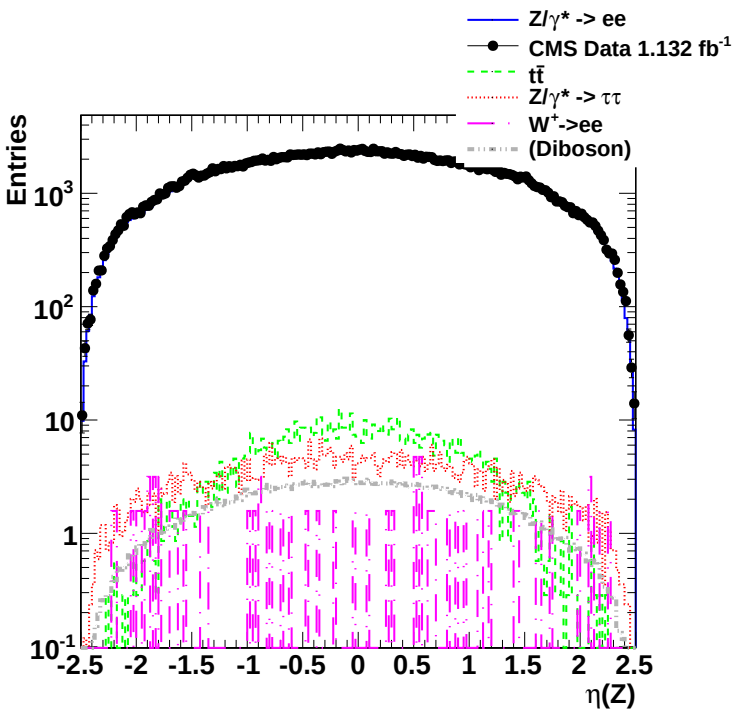

Figure 4.4: Pseudorapidity (η) distribution of Z bosons.

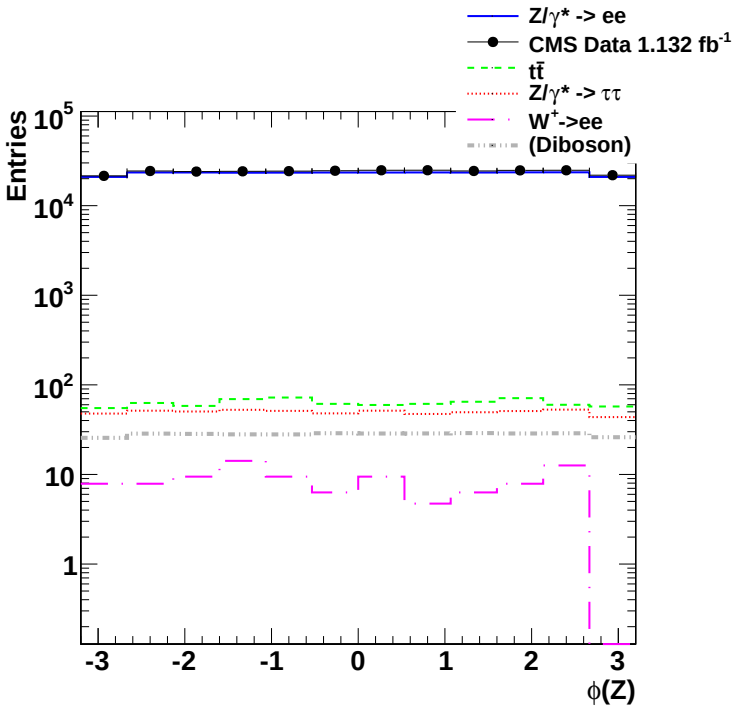

Figure 4.5: Azimuthal angle (ϕ) distribution of Z bosons.

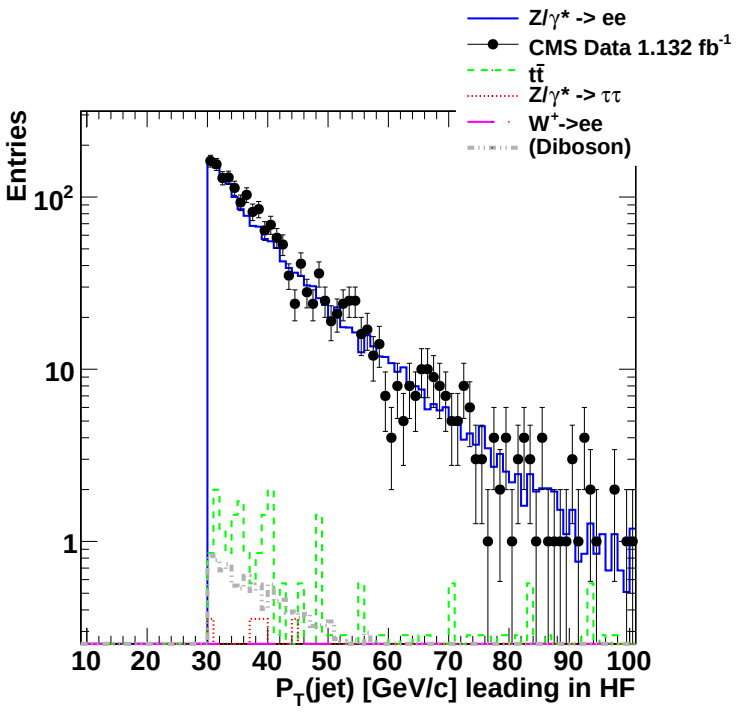

Figure 4.6: Transverse Momentum (P_T) distribution of leading jet in HF.

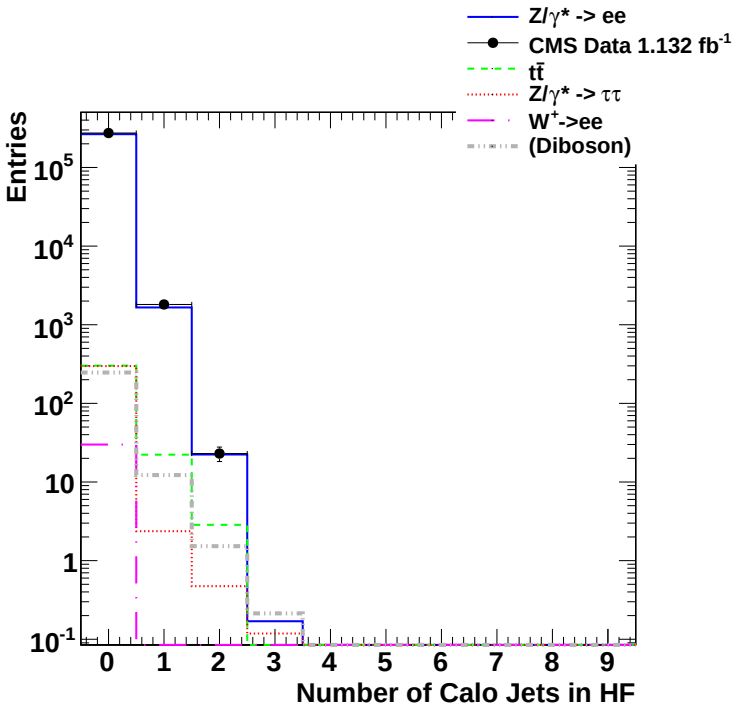

Figure 4.7: Number of jets in HF with transverse momentum greater than 30 GeV, accompanying Z candidates.

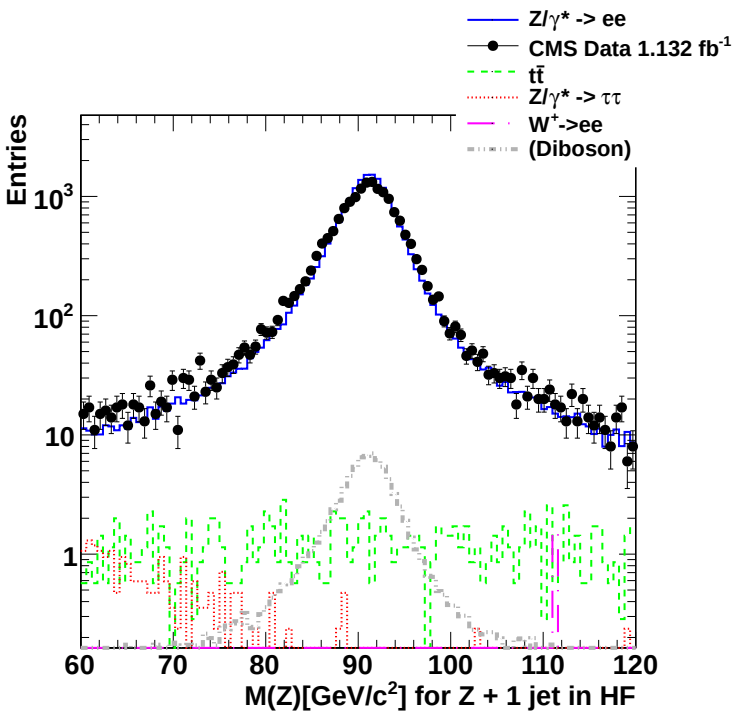

Figure 4.8: Z mass reconstructed from di-electrons for Z +1 jet events.

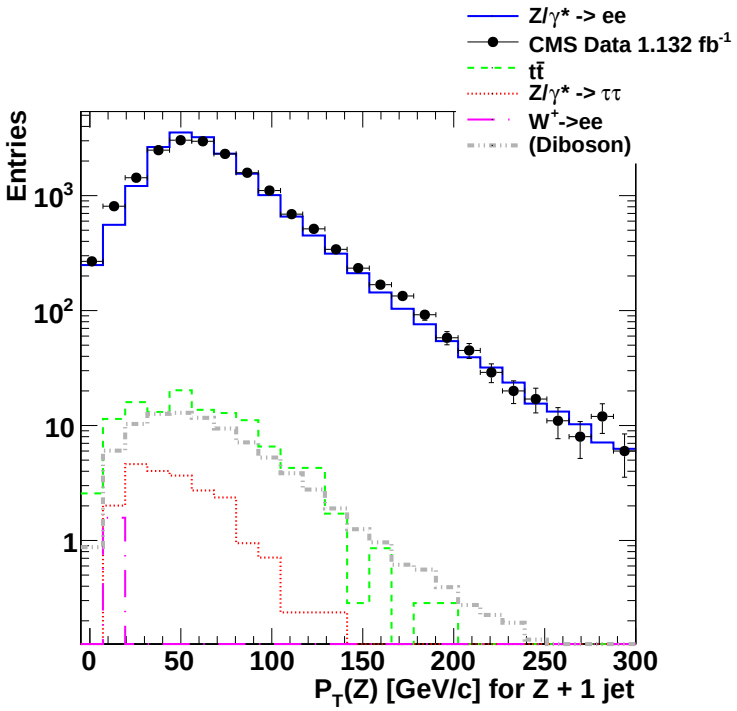

Figure 4.9: Z P_T reconstructed from di-electrons for Z +1 jet

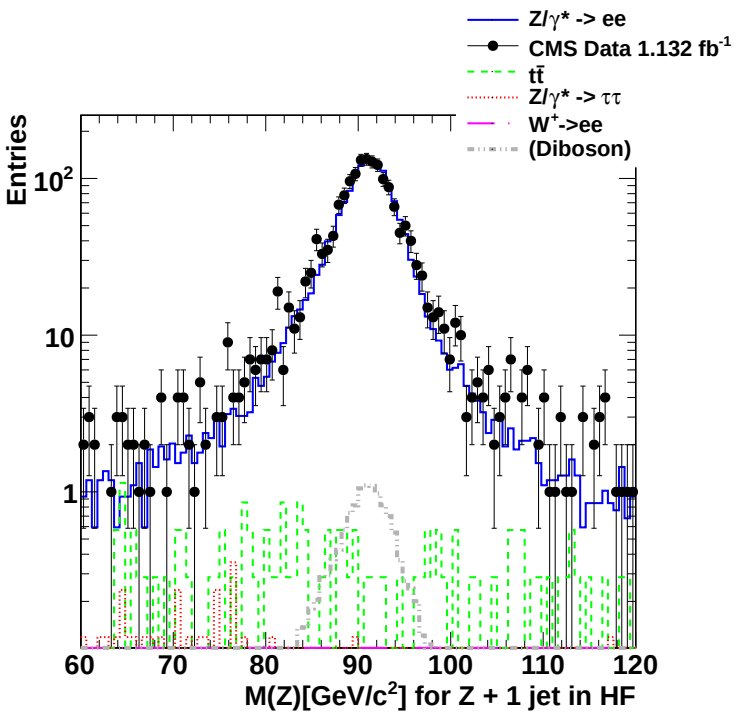

Figure 4.10: Z mass reconstructed from di-electrons for Z +1 jet (jet in HF).

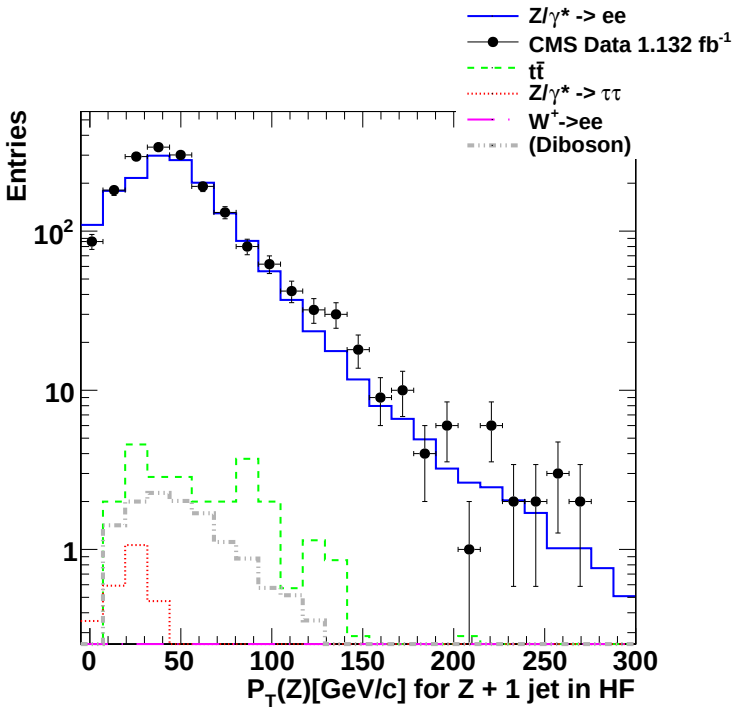

Figure 4.11: Z P_T reconstructed from di-electrons for Z +1 jet (jet in HF)

CHAPTER 5

CALIBRATION OF HCAL FORWARD CALORIMETER USING Z+JET EVENTS

5.1 The Method

In CMS experiment, there are many different ways to correct the jets [2], which aims to correct the measured energy of the jets with respect to the expected energy of the final state particle coming out of the interaction and forming the jet. The calorimeter tower responses are corrected firstly, using test beam data. Afterwards, there are different jet energy correction methods to correct the jets energy and also to remove some noise and pile-up effects.

Correcting the Forward Jets plays a crucial role in many aspects, in processes where precise calculation of Missing Energy is vital. For Higgs searches through the Vector Boson Fusion channel, precise measurement of the tagging jets in HF is important for the identification of the Higgs boson.

There are methods to correct the jet energy scale using QCD di-jet samples, but this will over-estime the jet scale in the Forward region [31]. Another method, correction of energy scale using Z→ee [32], where one electron is in the central region and the other in HF; aims to correct the Electromagnetic Fraction of energy in HF, namely the Long fiber hits using Z mass constraint.

The method proposed in this chapter aims to correct the jets overall energy scale, where the jets are in HF. Similar to the method presented in this chapter, γ + jet events can be used as they are used in Barrel and Endcap regions [33], but as the concerning range is the forward region, this method has more background so has more uncertainty regarding forward jets.

The Z + jet events shown in previous chapter are almost background free, and hence this event topology can be used for the energy scale correction of the jets especially in HF.

The method is based on the measurement of transverse momentum ratio of Z to the jet. For the analysis, exclusive 1 jet events lying in the mass window of 60 GeV < M(Z) < 120 GeV are taken. Z and jets are required to be back to back by restricting the $\Delta\phi(jet, Z) \geq 2.8$. The Z candidates are reconstructed from oppositely charged di-leptons.(For this part of the thesis, for completeness of the results, Z ($\mu\mu$) + jet channel is also included.) Since the Z and the jets are back to back on the transverse plane, the ratio of the Z pT to the jet pT can be used as a multiplicative calibration coefficient.

$$C_i = P_{T,Z}/P_{T,J_i} \tag{5.1}$$

One example Z + 1 jet event where the jet is in HF taken from CMS collision data is shown using CMS Fireworks visualization program in Figure 5.1. The red lines are representing the ECAL calorimeter hits created by electrons, and the GSF electrons are shown as blue lines. The yellow line represents the Calo jet with cone size of $\Delta R = 0.5$. As shown in the figure, the electrons coming from the Z candidate are in the central region, whereas the jet is in HF-. From the transverse view, it can be seen that the jet and the Z candidate are almost back-to-back.

There is not enough clean Z + 1jet events to make the measurement tower by tower with the existing data. Hence some towers are combined together in order to increase the statistics. The forward calorimeter is divided into three rapidity (η) ranges and for each of them the coefficients are measured. The rapidity ranges and the corresponding tower indices (also noted as $i\eta$) are given in Table 5.1.

Table 5.1: HF tower indices and corresponding eta ranges.

Tower Index	Low $\lvert\eta\rvert$	High$\lvert\eta\rvert$
29-30	2.853	3.139
31-32	3.139	3.489
33-41	3.489	5.191

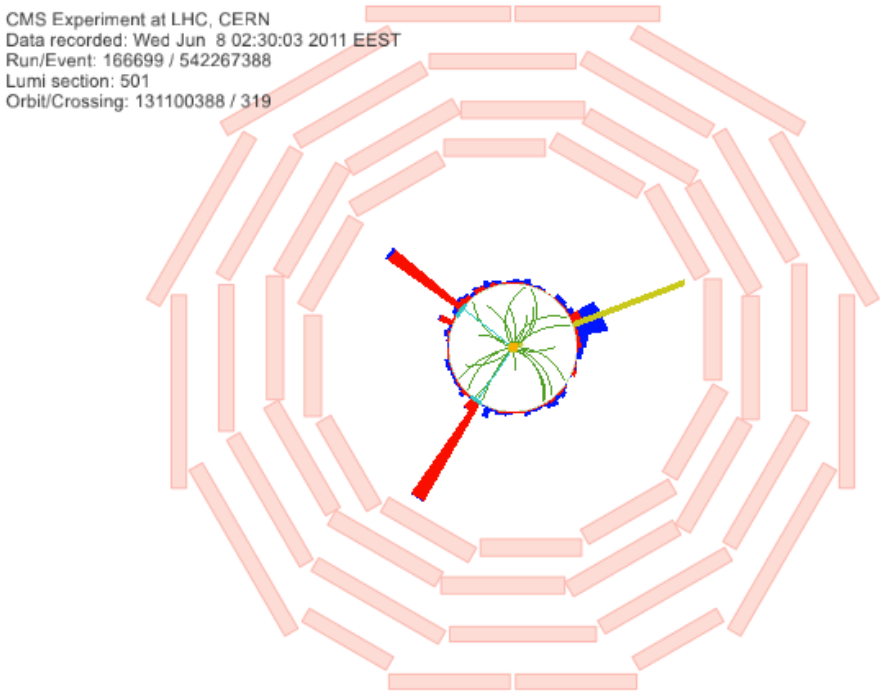

(a) transverse view

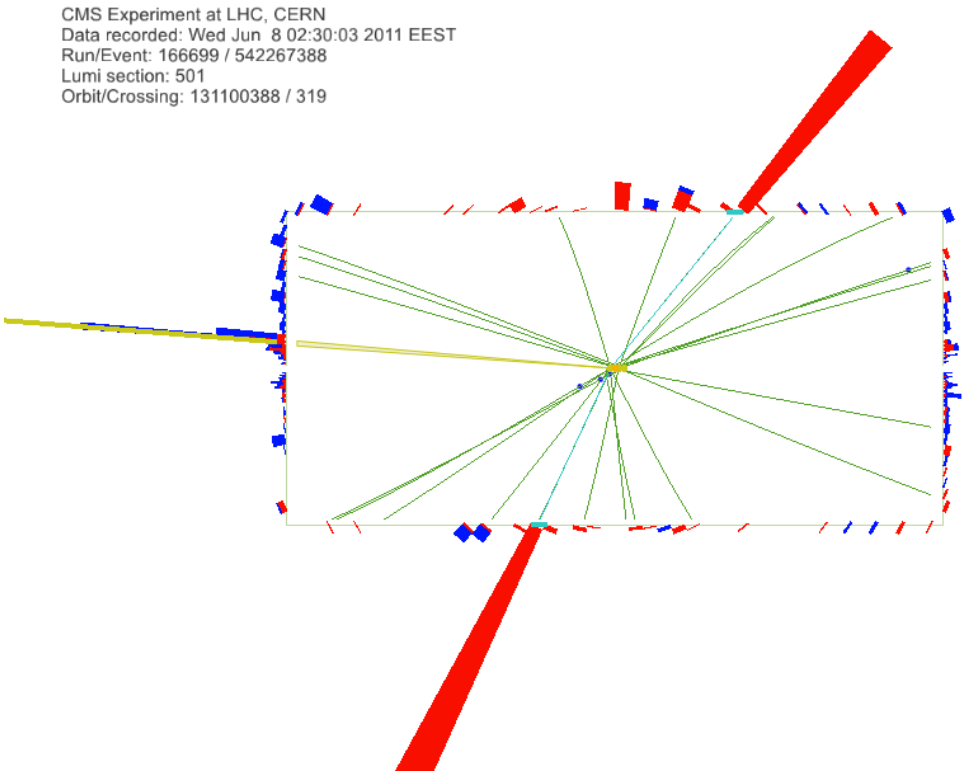

(b) $\rho - \phi$ plane view

Figure 5.1: Example Z + 1jet event from CMS Fireworks where jet is in HF.

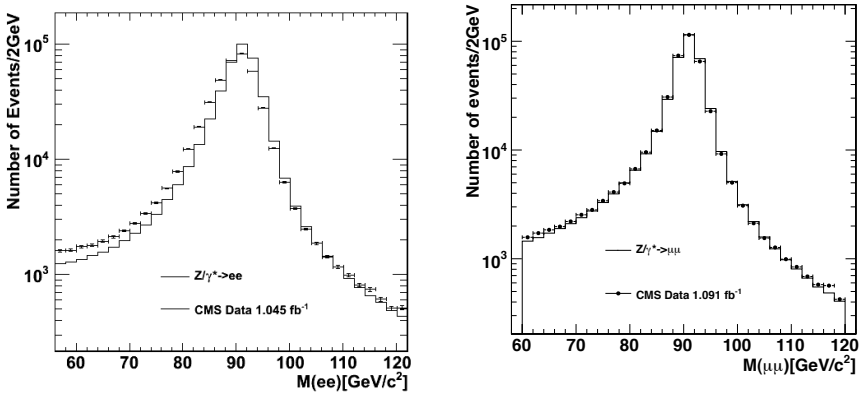

(a) (b)

Figure 5.2: Z mass in data and MC(Powheg) reconstructed from(a) di-electrons (b) di-muons. Backgrounds are small and not shown.

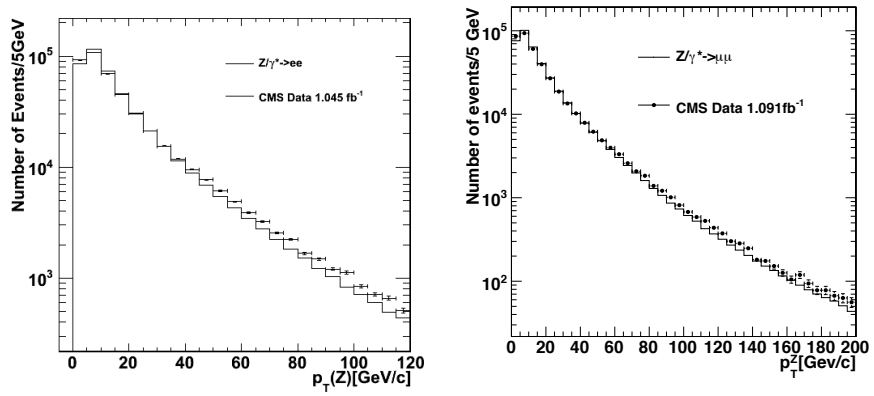

(a) (b)

Figure 5.3: Z Transverse Momentum in data and MC(Powheg) reconstructed from(a) di-electrons (b) di-muons. Backgrounds are not shown.

5.2 Correction Factors and Validation on WW sample

For each η-range given in Table 5.1, $P_{T,Z}/P_{T,J}$ ratio plots are displayed in Figure 5.5.

The correction factors obtained from electron and muon channels are summarized in the Table 5.2.

The correction factors obtained are tested on the WW + jets Monte Carlo sample. The W's decaying to a quark and an anti-quark are taken and the uncorrected Ak5Calo jets matched

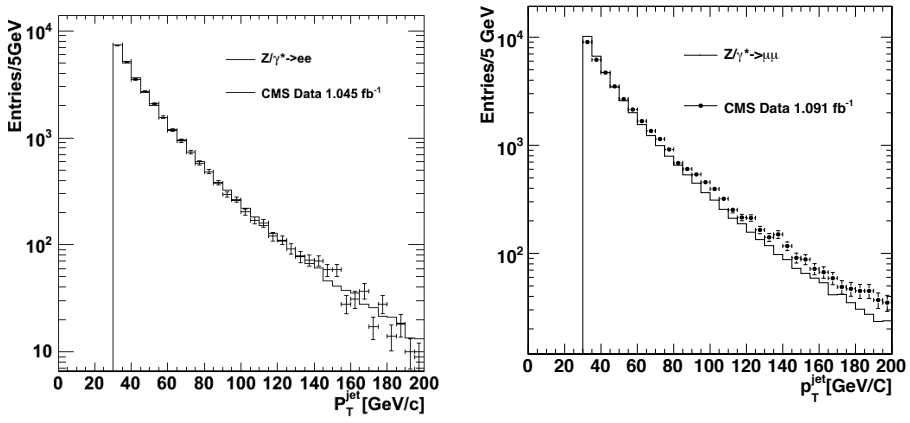

(a) (b)

Figure 5.4: Jet transverse momentum from(a) di-electron (b) di-muon channels in data and MC(Powheg). Backgrounds are not shown.

Table 5.2: Calibration coefficients derived from muon and electron channels.

HF Plus			
Tower Index	electron channel	muon channel	average
29-30	1.405	1.361	1.383
31-32	1.089	1.153	1.121
33-41	1.062	1.105	1.084
HF Minus			
Tower Index	electron channel	muon channel	average
29-30	1.308	1.337	1.323
31-32	1.188	1.193	1.191
33-41	1.114	1.146	1.130

to the gen-level quarks which come from the same W. Both of the jets originating from the W are restricted to $|\eta| > 2.853$. Each component of the 4-momentum of the matched jets are corrected by multiplying with the corresponding coefficients.

The invariant mass of the jets is calculated for the raw and the corrected jets. Figure5.6 shows the invariant mass distribution of the uncorrected and the corrected jets. The correction factors improves the W mass by 19% in the electron, and 22% in the muon channel. The W mass before correction is 64.1 GeV and after corrections the mean is 78.1 GeV for the muon and 76.1 GeV for the electron channel. The resolution is 20.6% before and $\sim$ 19% after the

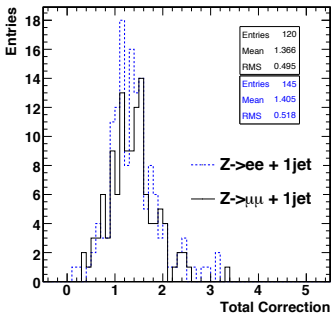

(a) +29< $i\eta$ <+30

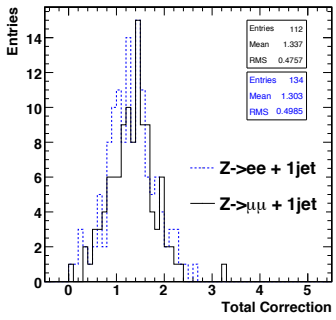

(b) -29> $i\eta$ >-30

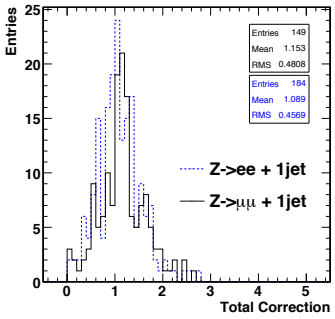

(c) +31< $i\eta$ <+32

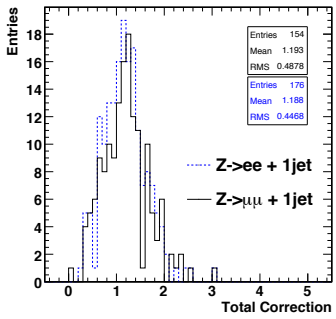

(d) -31> $i\eta$ >-32

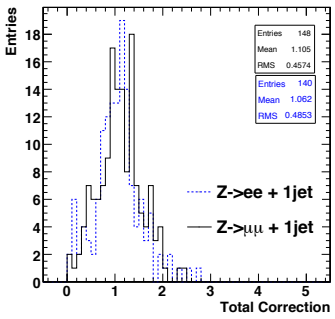

(e) +33< $i\eta$ <+41

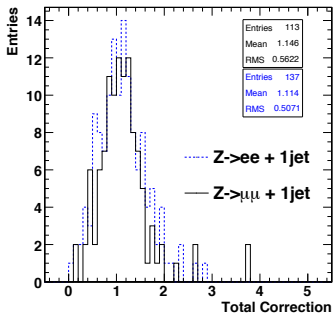

(f) -33> $i\eta$ >-41

Figure 5.5: P_Z^T/P_J^T ratios for the combined HF towers.

corrections for both channels.

$$
\begin{aligned}
E_J^{Corr} &= C_i \; E_J^{Raw} \\
P_{x,J}^{Corr} &= C_i \; P_{x,J}^{Raw} \\
P_{y,J}^{Corr} &= C_i \; P_{y,J}^{Raw} \\
P_{z,J}^{Corr} &= C_i \; P_{z,J}^{Raw}
\end{aligned}
\tag{5.2}
$$

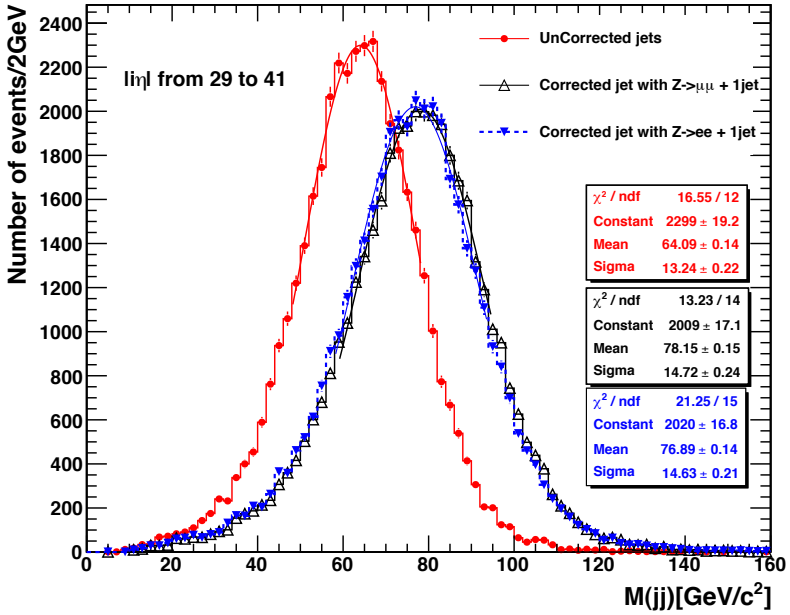

(a)

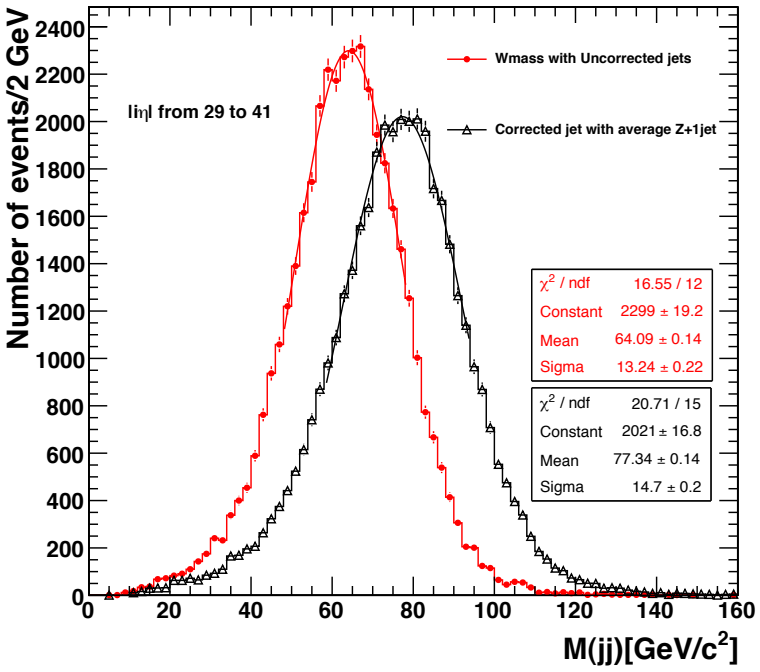

(b)

Figure 5.6: W mass from raw and corrected jets ; (a) separately for electron and muon channels, (b) and by the mean of the correction constants in each channel.

5.3 Z + Jet and Z(ee) corrections together (version 1)

It is possible to get Z + jet corrections on top of other corrections derived using $Z \rightarrow e^+ e^-$ in which one electron is in the tracker volume & the other is in HF. To achieve this, the correction factors obtained from Z(ee) method (the constants are preliminary results taken from Reference [32]) are first applied on the jets but only on the Long fibers of HF. The "Long energy fraction" is obtained by the following equation from the Hadronic and Electromagnetic Energy Fraction in HF for each jet assuming all the energy of the jet is concentrated at the central tower of the jet;

$$\begin{aligned} L(i) &= 0.5\ E^{HF}_{Had}(i) + E^{HF}_{EM}(i) \\ S(i) &= 0.5\ E^{HF}_{Had}(i) \end{aligned} \tag{5.3}$$

Where i is the tower index. The HF towers 29-31 on both sides are shaded by the HCAL Endcap Calorimeters, so the sum of $L + S$ is not equal to the total raw energy of the jet in that region. The profile plot shows the ratio of $L + S$ to Raw Energy of the jet with respect to the jet physical η in the WW sample.

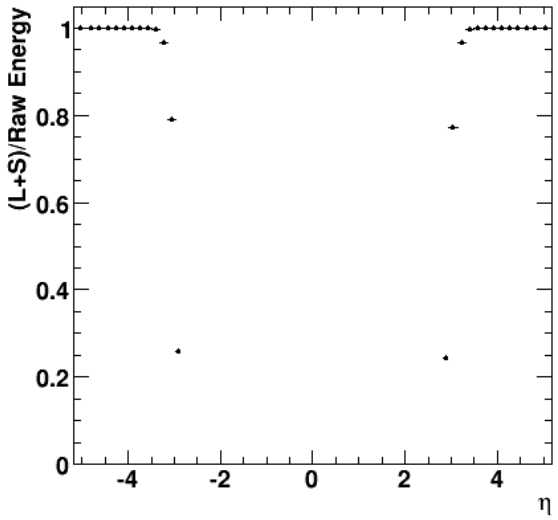

Figure 5.7: Ratio of Long + Short energy of the jet to the total jet raw energy versus jet rapidity (η).

The Z(ee) calibration constants are applied on the Long energy for towers 32-41 in the Z+Jet sample. Then, jet P_T is corrected with the correction factors obtained from Z(ee), and the ratio of Z transverse momentum to the Zee corrected jet transverse momentum is calculated. The ratio for different ranges are shown in Figure 5.8 and summarized in Table 5.3. The correction chain is summarized below.

$$
\begin{aligned}
E_J^{Zee} &= c\ L + S \\
c_1 &= E_J^{Zee}/E_J^{Raw} \\
c_{Z+j} &= P_{T,J}^{Zee}/(c_1\ P_{T,J}^{Raw})
\end{aligned}
\tag{5.4}
$$

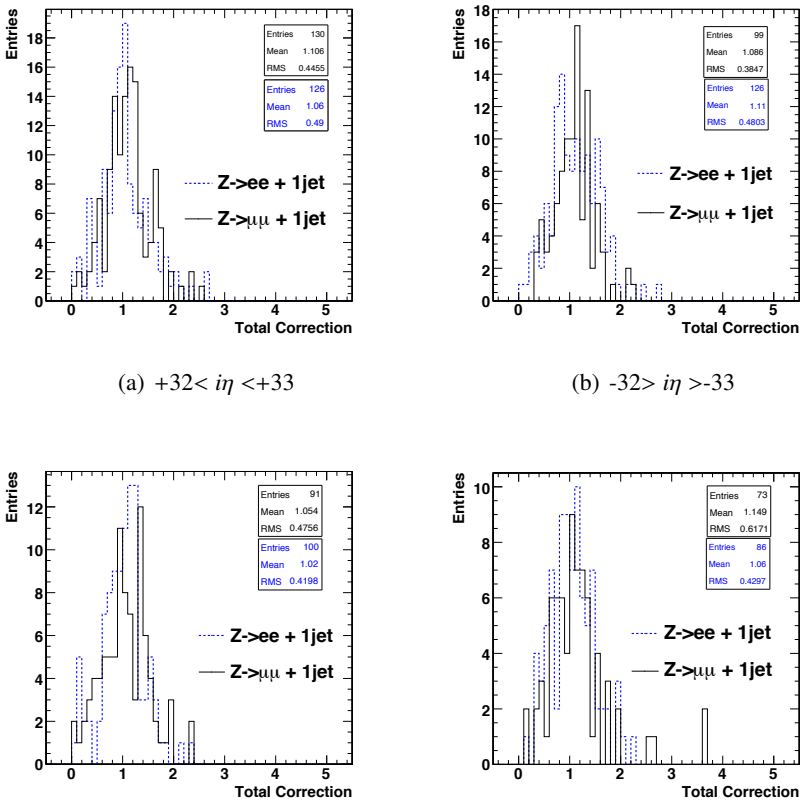

(a) +32< $i\eta$ <+33 (b) -32> $i\eta$ >-33

(c) +34< $i\eta$ <+41 (d) -34> $i\eta$ >-41

Figure 5.8: Correction factors obtained by taking Z(ee) corrections as a base set.

Then both of the corrections are applied on the jets in the WW sample. First Z(ee) correction factors are appied on the Long fibers and then on top of Z(ee) corrected jets, the constants

Table 5.3: Calibration coefficients for combined Z(ee) + Z+jet corrections (v1).

HF +			
Tower Index	electron channel	muon channel	average
32-33	1.060	1.106	1.083
34-41	1.020	1.054	1.037
HF -			
Tower Index	electron channel	muon channel	average
32-33	1.110	1.086	1.098
34-41	1.060	1.149	1.104

found from Z + jet events are applied. The invariant mass of jets from uncorrected and corrected jets is shown in Figure 5.9. This shows that it is possible to improve the scale if we begin with Zee corrected HF channels.

5.4 Z + Jet and Z(ee) corrections together (version 2)

The energy of the long fibers corrected using Zee events can be held fixed and the "short energy" scale can be derived using Z+jet events. The short fibers are corrected with the calibration coefficient shown in Equation 5.5.

$$C^s = \frac{P_Z^T / P_J^T \, (L + S) - C^{Zee} \, L}{S} \tag{5.5}$$

The correction factors are then validated using the WW sample. The Long energy is multiplied by the Zee corrections and the Short is multiplied by the factor obtained from Z+jet events.

$$\frac{C^{Zee} \, L + C^s \, S}{L + S} \tag{5.6}$$

The correction factors obtained are used to correct the 4-momentum of the jets. The correction factors are summarized in Table 5.4 and shown in Figure 5.10. The effect of the correction on W mass is shown in Figure 5.11. The W mass reconstructed using the corrected jets is much closer to the known W mass. It is important to note that the constants derived in this section are based on a sample with improved ϕ corrections.

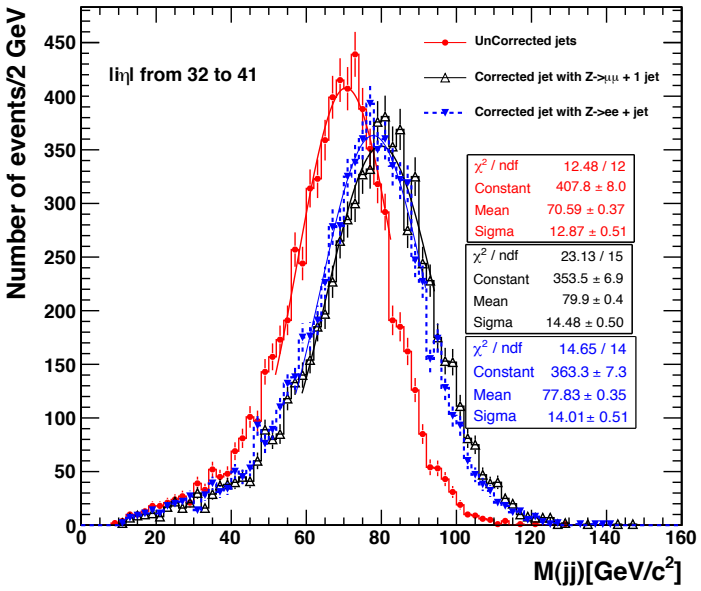

(a)

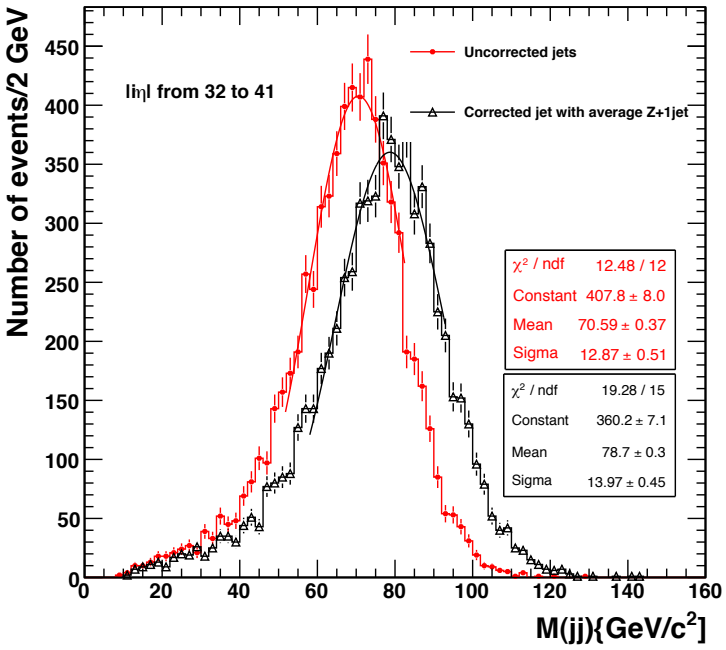

(b)

Figure 5.9: W mass from raw and corrected jets for Z(ee) + Z+jet correction (v1); (a) separately for electron and muon channels, (b) and by the mean of the correction constants in each channel.

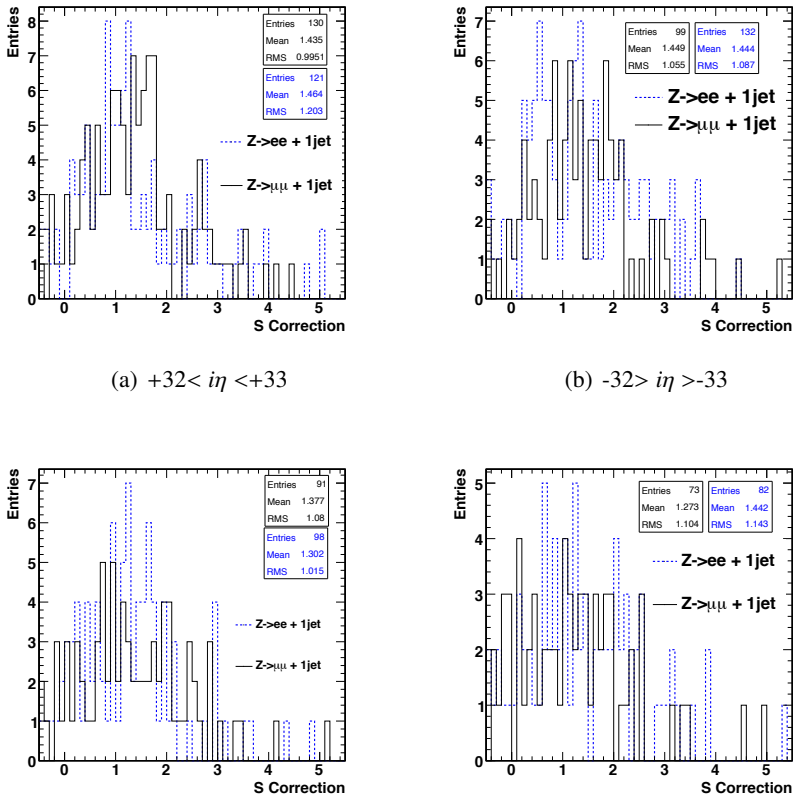

(a) +32< $i\eta$ <+33

(b) -32> $i\eta$ >-33

(c) +34< $i\eta$ <+41

(d) -34> $i\eta$ >-41

Figure 5.10: Z + Jet and Zee corrections together (Long Scale fixed useng Zee and Short scale from Z+Jets).

Table 5.4: Calibration coefficients for combined Z(ee) + Z+jet corrections (v2).

HF +			
Tower Index	electron channel	muon channel	average
32-33	1.464	1.435	1.449
34-41	1.302	1.377	1.34
HF -			
Tower Index	electron channel	muon channel	average
32-33	1.444	1.449	1.446
34-41	1.442	1.273	1.358

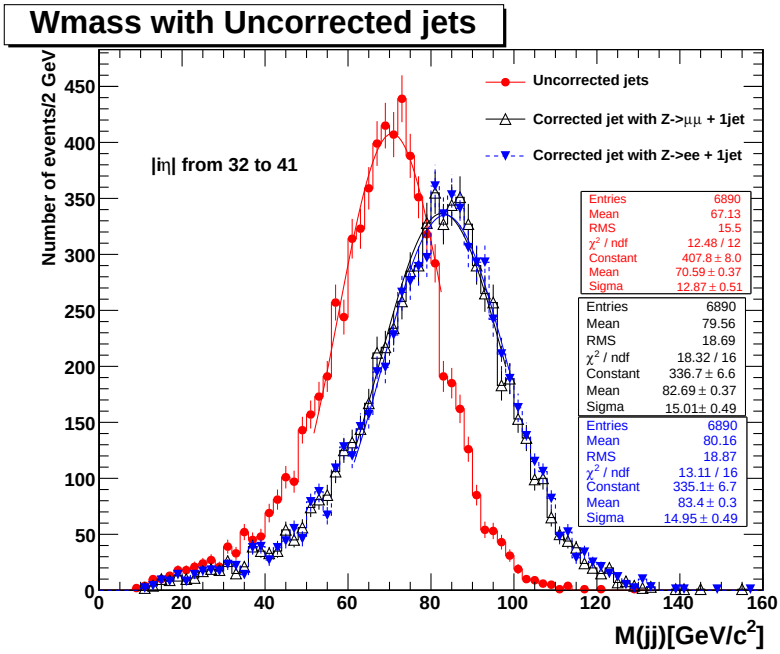

(a)

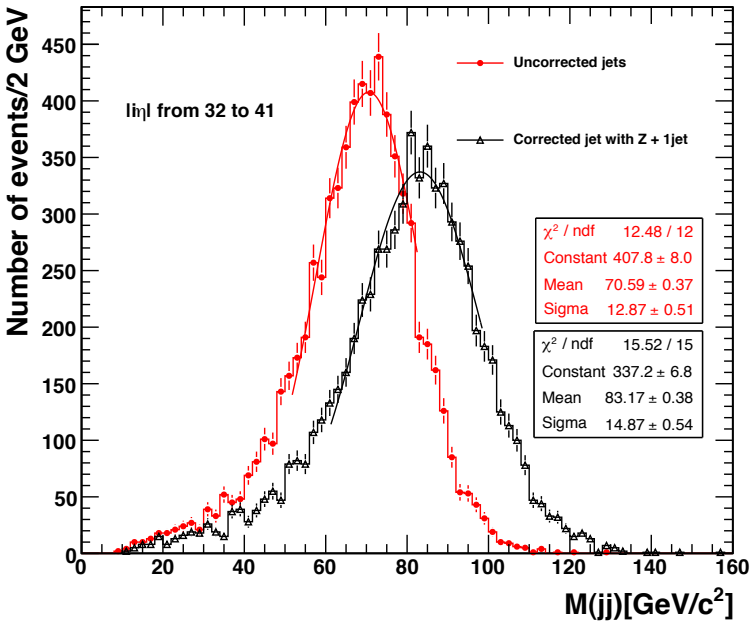

(b)

Figure 5.11: W mass from raw and corrected jets for Z(ee) + Z+jet correction (v2); (a) separately for electron and muon channels, (b) and by the mean of the correction constants in each channel.

Pile-Up Effect on the Calibration Constants

Pile-up in collision terminology stands for the extra collisions which occurs during bunch crossing. When an event is recorded by the CMS detector, not all of the physical objects originate from the same vertex, i.e. jets may originate from another pair of protons colliding at the same time. The number of primary vertices is a measure of the number of pile-up collisions in that event.

A simple analysis is carried out to understand the effect of pile-up on the calibration constants. In the Drell-Yan Monte Carlo sample, we chose those events with one primary vertex only, and measured the P_Z^T/P_J^T for those events and also for all events in the same MC sample. Then, to observe the effect of pile-up, we took the ratio of constants of Number of Primary Vertices ($PV = 1$) events to all events as shown in Equation 5.7.

$$\begin{aligned} C_1^{PV1} &= P_{T,Z}^{PV1}/P_{T,J}^{PV1} \\ C_1^{all} &= P_{T,Z}^{all}/P_{T,J}^{all} \\ C_2 &= C_1^{PV1}/C_1^{all} \end{aligned} \tag{5.7}$$

Then the pile-up correction factor derived from MC is multiplied by the correction factors driven from the data. The obtained correction factors are summarized in Table 5.5.

Table 5.5: Calibration coefficients forZ+jet with pileup corrections applied.

HF +	
Tower Index	electron channel
29-30	1.4827
31-32	1.1560
33-41	1.2285
HF -	
Tower Index	electron channel
29-30	1.4222
31-32	1.2648
33-41	1.1845

These correction factors are applied on the jets in WW sample. The effect of the new corrections is shown in Figure 5.12. W mass is again restored but, as expected, it is 3-4 GeV higher than the W mass obtained from corrected jets without pile-up corrections.

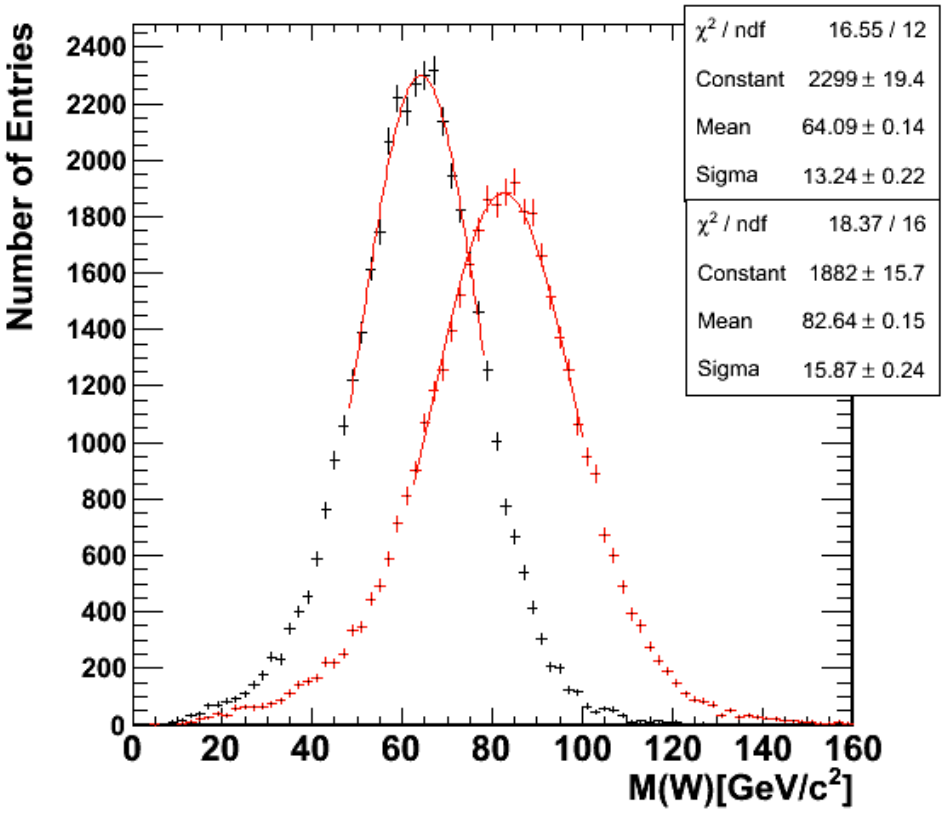

Figure 5.12: W mass from pile-up corrected coefficients derived from electron channel only.

CHAPTER 6

CONCLUSIONS

The Large Hadron Collider (LHC) machine at CERN is providing collisions since the end of 2009, producing data for physics analysis. CMS, being one of the LHC experiments, focuses on variety of physics topics. Standard Model and theories beyond the Standard Model are being tested by the CMS experiment. To carry out precise measurements regarding these topics, it is important to make exact measurement of jets ant their physical variables. Hence, correction of forward jets is vital for many physics processes at the CMS experiment at LHC.

In this thesis, an application of the method based on using well balanced Z + 1 jet events for calibrating the HF is presented. The calibration work carried out is also presented in the CMS Detector Note DN -2011/009 [4]. The samples used are taken from $\sim$1.1 fb^{-1} integrated luminosity of proton proton collisions recorded by the CMS experiment. The Z + jet events are almost background free, and hence is a reliable method for the jet energy scale corrections for the jets in HF.

Corrections are derived for three different rapidity bins for Calo-Jets in HF using the momentum balance of the Z boson to the raw jet.

It is verified that the proposed method can be applied jointly with Z(ee) driven corrections [32] derived uzing the Z mass constraint. Two different versions regarding combined application of the methods is carried out.

- The long fiber hits are corrected with Z(ee) driven corrections, and the overall jet scale is corrected with the tranverse momentum ratio of Z boson to the Z(ee) corrected jet.

- The long fiber hits are corrected with Z(ee) driven corrections, and a method is provided

to correct the short energy fraction.

A simple test is also carried out to understand the effect of pile-up on the calibration coefficients. A simple method is proposed to eliminate the effect of pile-up.

The correction factors derived from all proposed techniques are then tested on a WW sample using the W-mass constraint. It is shown that the corrections applied on Calo-Jets improved the W mass by ~20 % for both channels without loss of resolution. Corrections factors obtained are shown to be applicable either as a correction on each calorimeter hit, or as an overall jet energy scale correction.

The Z + jet event samples provide almost background free measurements, but they are poor in statistics. As more data is collected by the CMS experiment, this method can give more accurate correction factors, where the HF can be divided into smaller rapidity bins. Also, once with more data, the tighter cut set regarding the electrons (WP 80) can be used once more data is available to have more precise results.

REFERENCES

[1] The CMS Collaboration, CMS Physics Technical Design Report Vol 2. CERN/LHCC 2006-021,2006.

[2] K. Mishra, Plans for Jet Energy Correction at CMS. University of Chicago, 2009.

[3] The CMS Collaboration. Determination of the jet energy scale using Z $\rightarrow$ e^+e^- + Jet P_T balance and a procedure for combining data driven corrections. CMS PAS JME-09-005,2009.

[4] N. Akchurin, K. Kovitanggoon, E. Yazgan, B. Bilin, M. T. Zeyrek, Forward Jet Energy Correction with Z+Jet Events. CMS DN -2011/009, 2011.

[5] D.Griffiths, Intro. to Elementary Particles. John Wiley and Sons, 1987.

[6] D. H. Perkins, Intro. to High Energy Physics. Cambridge Uni. Press, 2000.

[7] Particle Data Group, The Review of Partice Physics Journal of Physics G, 2010.

[8] O.S. Bruning et. al, LHC Design Report. CERN-2004-003-V-1, 2004.

[9] LHCb Muon Group Home Page, http://lhcb-muon.web.cern.ch/lhcb-muon/figures/, last accessed on 22/08/2011.

[10] The CMS Collaboration, CMS Physics Technical Design Report Vol 1. CERN/LHCC 2006-001, 2006.

[11] Transverse Slice of the Compact Muon Solenoid (CMS) Detector, https://cms-docdb.cern.ch/cgi-bin/PublicEPPOGDocDB/RetrieveFile?docid=97&version=1&filename=CMS_Slice_elab.swf, last accessed on 30/08/2011.

[12] http://cms.web.cern.ch/cms/Detector/FullDetector/index.html, last accessed on 24/08/2011.

[13] The CMS Collaboration, CMS Tracker Technical Design Report. CERN/LHCC 98-6, 1998.

[14] The CMS Collaboration, CMS ECAL Technical Design Report. CERN/LHCC 97-33, 1997.

[15] The CMS Collaboration, CMS HCAL Technical Design Report. CERN/LHCC 97-31, 1997.

[16] The CMS Collaboration, Design, performance, and calibration of CMS forward calorimeter wedge. Eur. Phys. J. C 53, 139-166, 2008.

[17] The CMS Collaboration, CMS The Magnet Project Technical Design Report. CERN/LHCC 97-10, 1997.

[18] The CMS Collaboration, CMS The Muon Project Technical Design Report. CERN/LHCC 97-32, 1997.

[19] The POWHEG BOX, http://powhegbox.mib.infn.it/, last accessed on 01/09/2011.

[20] PYTHIA 8.1, http://home.thep.lu.se/ torbjorn/Pythia.html, last accessed on 30/08/2011.

[21] GEANT 4, http://geant4.cern.ch/, last accessed on 04/09/2011.

[22] The CMS Collaboration, The TriDAS Project, Technical Design Report, Volume 1: The Trigger Systems. CERN / LHCC 2000 - 38, 2000.

[23] V. M. Ghete, The CMS L1 Global Trigger Offline Software. http://www.hephy.at/fileadmin/user_upload/Vortraege/L1offlineSW_Ghete.pdf

[24] Data Formats and Data Tiers, https://twiki.cern.ch/twiki/bin/view/CMSPublic/WorkBookDataFormats, last accessed on 30/08/2011.

[25] ROOT, http://root.cern.ch/drupal/, last accessed on 03/09/2011.

[26] Hung-Liang Lai et. al., New parton distributions for collider physics. arXiv:1007.2241[hep-ph], 2010.

[27] Baffioni S.et. al., Electron reconstruction in CMS. THE EUROPEAN PHYSICAL JOURNAL C, page 1099 1116, 2007.

[28] W. Adam et. al., Reconstruction of electrons with the gaussian-sum filter in the CMS tracker at the LHC. CMS Note, 2005.

[29] Martijn Mulders, Muon Reconstruction and Identification in CMS. (10^{th}) Topical Seminar on Innovative Particle and Radiation Detectors, 2006.

[30] M. Cacciari, G. P. Salam, and G. Soyez, The anti-kt jet clustering algorithm JHEP 04 (2008) 063, 2008.

[31] A. Nikitenko et. al., CMS Analysis Note-2010/004, 2010.

[32] Jeremiah Mans, HF Calibration with Z Electrons Update. https://indico.cern.ch/getFile.py/access?contribId=5&resId=0&materialId=slides, last accessed on 08/09/2011. &confId=148952

[33] The CMS Collaboration. Jet energy calibration with photon+jet events. CMS PAS JME-09-004, 2009.